Available online at www.sciencedirect.com
SCIENCE DIRECT®
ELSEVIER
International Journal of Solids and Structures 43 (2006) 855–886
INTERNATIONAL JOURNAL OF SOLIDS and STRUCTURES
www.elsevier.com/locate/ijsolstr

Elastic interaction of multiple delaminations in plates subject to cylindrical bending

Martin G. Andrews [a], Roberta Massabò [b,*], Brian N. Cox [c]

[a] *Department of Civil and Environmental Engineering, Northwestern University, Evanston, IL 60208, USA*
[b] *Department of Structural and Geotechnical Engineering, University of Genova, Genova 16145, Italy*
[c] *Rockwell Scientific Co., Thousand Oaks, CA 91360, USA*

Received 14 October 2004; received in revised form 8 April 2005
Available online 15 June 2005

Abstract

This paper deals with the elastic interaction of multiple through-width delaminations in laminated plates subject to static out of plane loading and deforming in cylindrical bending. A model has been formulated utilizing the classical theory of the bending of beams and plates and accounting for non-frictional contact along the delamination faces. Strong interaction effects arise between the delaminations including shielding and amplification of the energy release rate and modification of the mode ratio as compared to a structure with only a single delamination. Such behavior has been summarized in maps that completely characterize the response of a system of two delaminations in a cantilever beam. The quasi-static propagation of the system of delaminations is also strongly controlled by the delamination interactions, which lead to local snap-back and snap-through instabilities, crack arrest and crack pull-along. The results show similarity to those for cracked infinite bodies, but the finite-thickness of the plate plays an important role and gives rise to more complex behaviors. The stability of the equality of length of a system of n delaminations is controlled by their spacing. Finite element calculations confirm that the model proposed here is accurate, except when the difference in the length of the interacting delaminations is less than a few times the separation of their planes.

Keywords: Multiple delamination; Shielding; Amplification; Crack interaction; Laminated structures

1. Introduction

Due to poor interlaminar properties, laminated fiber reinforced composites are susceptible to delaminations caused for instance by manufacturing errors, edge effects or by such in service situations as impact,

* Corresponding author. Tel.: +39 010 353 2956; fax: +39 010 353 2534.
E-mail address: massabo@diseg.unige.it (R. Massabò).

0020-7683/$ - see front matter © 2005 Elsevier Ltd. All rights reserved.
doi:10.1016/j.ijsolstr.2005.04.025

monotonic and cyclic loading. In the case of impact, typically many delaminations occur between layers of different fiber orientation. The presence of the delaminations is often undetectable on the surface and may significantly reduce the stiffness and load carrying capacity of the structure (Pavier and Clarke, 1995). When a load is applied that causes sufficient interlaminar stresses, the delaminations may grow, often catastrophically, separating the structure into two or more pieces and causing further reduction in stiffness and/or failure. While the behavior of structures in the presence of a single delamination has been widely studied since the early work of Kanninen (1973, 1974) and others (see Massabò and Cox, 1999; Sridhar et al., 2002 for work of the authors), the problem of the multiple delamination of laminated structures is not yet fully understood. This paper examines the interaction of multiple delaminations in plates subject to static out of plane loading and the effects this interaction has on the fracture behavior and structural response of the laminate, using a cantilever plate as a case study.

An important interaction effect is contact that may occur between the delaminated plies. When there are multiple delaminations, studies, such as those dealing with structures subject to in plane loadings (Larsson, 1991; Suemasu, 1993), have shown that extensive contact may occur along the delaminations faces. Contact significantly affects the critical energy release rate for the extension of a delamination. Contact also introduces regions in which friction may be important. The presence of contact will be shown later not to be limited to delaminated structures subject to in-plane loading.

The effect of the interaction of the delaminations on the energy release rates is another important phenomenon. Larsson (1991), using a model based on the theory of bending of plates to study delaminated plates under in-plane loading, observed a discontinuity in the energy release rate of a delamination when its length is equal to the length of other delaminations of the system. This discontinuity was thought to be an anomalous product of the assumptions of plate theory; however, this paper will show that the discontinuity well approximates the actual behavior. Zheng and Sun (1998) showed that the effect of the interactions between delaminations on the energy release rates depends on the through-thickness distance between the delaminations. For the structure and crack configurations that they studied, they also observed that the presence of a smaller delamination has little effect on the energy release rate of a delamination, while the presence of a longer delamination may induce strong amplification or shielding. This paper will show that in more general crack configurations, the presence of short delaminations may also strongly affect the response.

The interaction effects also influence the stability of the equality of length of a system of n delaminations. As it will be shown later, the delaminations of a stable system will tend to grow together, leading to an increased capacity of the system to absorb energy and a more ductile structural response. An unstable system of delaminations will have more localized delamination growth of only one or a small number of delaminations, leading to reduced energy absorption and a less ductile response. Suemasu and Majima (1996) showed that an axisymmetric system of equally spaced, equal size, penny-shaped delaminations in a clamped circular plate subject to a concentrated static force is stable. More general conclusions on the stability of systems of delaminations with unequally spaced cracks will be presented in the following.

The model proposed in this paper is based on the theory of bending of beams and plates and examines a multiply delaminated plate subject to static, out of plane loading and deforming in cylindrical bending. Non-frictional contact along the delamination surfaces is accounted for utilizing three approximations, two of which allow closed form solutions of the problem. The energy release rate and the stress intensity factors at each delamination crack tip are determined by the application of methods developed for beams and plates with a single delamination. The results are quantified for the case of a cantilever beam with multiple edge delaminations. Shielding and amplification of the energy release rates of the cracks and the interaction effects on the macro structural response of the plate are examined. The model is validated through finite element analyses.

2. Theoretical model

2.1. Model assumptions

The problem under consideration is a thin laminated plate of thickness h with n through width delaminations. A system of Cartesian coordinates x–y–z is introduced. Each delamination, with index i, is arbitrarily distributed across the thickness, with through-thickness position y_i and length a_i. The plate is subject to out of plane loading. An exemplary plate, with an applied surface pressure q, is shown in Fig. 1a.

The material comprising the plate is assumed to be homogeneous, isotropic and linear elastic, with elastic modulus E and Poisson's ratio v. The model is applicable to all laminates composed of isotropic layers of the same material. With modifications to account for different material properties in the through thickness direction, the model can also be applied to quasi-isotropic laminates and specially orthotropic laminates (i.e. laminates composed of layers whose principal material directions are aligned with the reference axes) with a large number of layers.

Only small deformations of the plate are considered, and plane strain conditions are assumed parallel to the x-y plane so that the plate deforms in cylindrical bending. Therefore, the governing equations of the plate correspond to those of a beam with a reduced Young's modulus $\overline{E} = E/(1 - v^2)$, where E is the longitudinal modulus. In the following analysis, the designation of beam and plate are identical. The classical theory of bending of beams, which neglects shear deformation, is utilized to determine the response of the delaminated structure.

The plate shown in Fig. 1a, is decomposed into multiple uncracked beam segments, defined by the coordinates of the crack tips and continuity conditions are applied at the cross sections separating beam segments. For purposes of notation, the beam segments are numbered from top to bottom and left to right in the structure, and delaminations are numbered from top to bottom. The height of beam segment k is h_k and its cross sectional moment of inertia and area are I_k and A_k, respectively. The generalized displacements of the centroidal axis of beam segment k are the axial and transverse displacements u_k and w_k, and the bending rotation φ_k. The stress resultants per unit width are axial force N_k, shear force V_k and bending moment M_k (Fig. 1b).

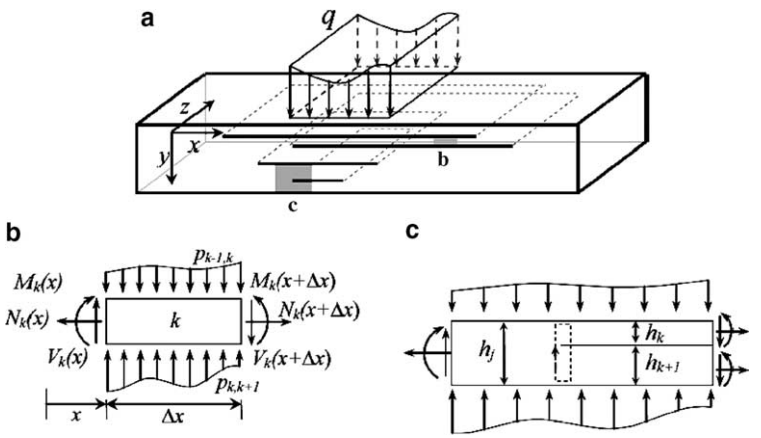

Fig. 1. (a) Exemplary plate with multiple through width cracks subject to transverse loading. (b) Equilibrium of a beam segment, showing stress resultants and contact pressures. (c) Crack tip element separating beam segments identified by j, k and $k+1$. The dashed line is the path used for calculating the J integral.

Assuming no shear deformation, $\gamma_k = 0$, the compatibility equations for the beam segment k are

$$\varphi_k = -w_{k,x}, \quad \varepsilon_k = u_{k,x}, \quad \kappa_k = \varphi_{k,x}, \tag{1}$$

where ϵ_k is the axial deformation and κ_k is the bending curvature and, x denotes differentiation with respect to the longitudinal coordinate x. The constitutive equations are

$$M_k = EI_k\kappa_k = -EI_k w_{k,xx}, \quad N_k = EA_k\varepsilon_k = EA_k u_{k,x}, \tag{2}$$

Equilibrium of the beam segment is given by:

$$M_{k,x} - V_k = 0, \quad V_{k,x} + p_{k,k+1} = p_{k-1,k}, \quad N_{k,x} = 0, \tag{3}$$

where $p_{k,k+1}$ and $p_{k-1,k}$ are either externally applied pressures or contact pressures acting on the lower and upper surfaces of the segment (Fig. 1b).

At the ith crack tip, Fig. 1c, with coordinate $x = x_i$ separating the beam segments j, k and $k+1$, the kinematic and static continuity conditions are

$$\begin{aligned}
&u_j + \frac{1}{2}(h_j - h_k)w_{j,x} = u_k, \quad u_j - \frac{1}{2}(h_j - h_{k+1})w_{j,x} = u_{k+1},\\
&w_j = w_k = w_{k+1},\\
&w_{j,x} = w_{k,x} = w_{k+1,x},\\
&N_j = N_k + N_{k+1},\\
&M_j = M_k + M_{k+1} - \frac{1}{2}(h_j - h_k)N_k + \frac{1}{2}(h_j - h_{k+1})N_{k+1},\\
&V_j = V_k + V_{k+1}.
\end{aligned} \tag{4}$$

The bending rotations of the beam segments at the crack tips, often referred to as root rotations, have been assumed in (4) to be identical to one another.

In the plate shown in Fig. 1a, depending on the loading conditions and the geometry of the delamination system, contact along the delamination surfaces may occur. This contact is assumed to be non-frictional, which allows free sliding along the surfaces of a delamination, and is represented by the contact pressures, $p_{k,k+1}$ and $p_{k-1,k}$. The presence of contact is simulated in three ways.

The first method is to assume that the deflections of the beams in the delaminated regions are the same. Interpenetration along the delamination surfaces is then avoided; however, the beam segments in the delaminated region are also constrained from separating from each other, thus preventing any opening along the delamination surfaces that may occur. This is referred to as the *constrained-contact* model and introduces the constraint equation $w_k = w_{k+1}$ between the delamination surfaces of beam segments k and $k+1$.

The second method is to assume no contact interaction between the beam segments in the delaminated region. This allows opening along the delamination surfaces; however, interpenetration can occur, $w_k \neq w_{k+1}$. This is referred to as the *unconstrained-contact* model.

The final method is to consider elastic contact along the delamination surfaces. The elastic contact is approximated using a Winkler foundation of linear springs, which represent the through-thickness stiffness of the contacting beam segments and act to resist interpenetration along the delamination surfaces. The stiffness of the springs for a contacting beam segment k is determined by considering one dimensional tension or compression of a beam element of height $h_k/2$. This model neglects shear deformations in the beam segment, which would lead to coupling of the springs (see Kerr (1964) for an in-depth discussion of foundation models), in accordance with what has been assumed initially. The stiffness of the layer of springs representing contact between two beam segments, k and $k+1$, is given by:

$$k_{k,k+1}(x) = H(w_k(x) - w_{k+1}(x))\frac{2E_T}{h_k + h_{k+1}}, \tag{5}$$

where E_T is the through-thickness modulus of the material ($E_T = E$ for an isotropic material) and $H(\cdot)$ is the Heaviside step function, $H(\xi) = \{1,\xi > 0;0,\xi < 0\}$, which ensures that the springs resist only interpenetration and do not resist opening between beam segments. The pressure exerted at the bottom and top of beam segments k and $k+1$ then follows as:

$$p_{k,k+1}(x) = k_{k,k+1}(x)(w_k(x) - w_{k+1}(x)). \tag{6}$$

This method is referred to as the *spring-contact* model. Since the regions of contact and opening are generally not known a priori, the problem in this case becomes nonlinear.

It will be shown in the following that the *constrained-* and *unconstrained-contact* models define upper and lower bound solutions of the *spring-contact* model. Both models can be recovered from the *spring-contact* model by taking the appropriate limit of the spring stiffness in Eq. (5). For the *constrained-contact* model, the limit $k_{k,k+1} \to \infty$ results in the constraint equation already defined, $w_k = w_{k+1}$. For the *unconstrained-contact* model, the limit as $k_{k,k+1} = 0$ results in $p_{k,k+1}(x) = 0$, namely the absence of any contact pressure. The *constrained-*and *unconstrained-contact* models, while less accurate than the *spring-contact* model, have the advantage of leading to closed form solutions of the problem in cases that require a numerical solution when treated with the *spring-contact* model. The solutions obtained with the simplified models are qualitatively similar to those of the *spring-contact* model and they can lead to insightful conclusions.

The proposed model relies on the three simplifying assumptions of zero shear deformation, absence of relative beam root rotations at the crack tips and non-frictional contact. The influence of shear deformation on the solution of single delamination problems is known to affect only quantitative details of the solution and to be negligible if the delamination is sufficiently long. In multiple delamination problems a stronger effect is expected when the delamination tips are close. However, current studies (Andrews et al., 2005) show that this effect is not strong in the absence of contact near the delamination tips and is negligible compared to the effect of unequal beam rotations at the delamination tips in the presence of contact.

The influence of the assumption of equal beam rotations at the crack tips has been shown previously to affect only quantitative details of the solution for single delaminations, leading to limited underestimation of the compliance of the system and the energy release rate for mode I fracture problems and to negligible effects in mode II fracture problems. In the presence of multiple delaminations the effect of the assumption is expected to be stronger due to the presence of contact between the crack faces. Different methods for correcting root rotations have been proposed since the early work of Kanninen (1973, 1974) (see for instance Williams, 1989; Sun and Pandey, 1994, Pandey and Sun, 1996; and Wang and Qiao, 2004). All methods, however, complicate the solution of the problem and as the crack interaction effects examined in this work will arise independently of the quantitative details of crack face phenomena, a simpler level of approximation has been utilized for this work.

Accounting for the presence of friction between the crack surfaces does not complicate the model greatly and could lead to interesting alterations of the results presented in this paper for certain geometries. This effect is not studied here and is the topic of current work (Andrews et al., 2005). The assumptions of the model and their implications will be discussed further in Section 5.

2.2. Model solution

An arbitrary section of the beam shown in Fig. 1a may be intersected by m of the n delaminations in the beam. Using the compatibility, equilibrium and constitutive equations defined above, the governing differential equations for the beam segments intersected by the section are

$$EI_k w_{k,xxxx} + p_{k,k+1} = p_{k-1,k}, \quad k = 1,\ldots,m+1, \tag{7}$$

$$EA_k u_{k,xx} = 0, \quad k = 1,\ldots,m+1, \tag{8}$$

where the p's are contact pressures between the beams, except for $p_{0,1}$ and $p_{m+1,m+2}$ which are externally applied pressures on the external surfaces of the section. Eq. (8), referring to the axial displacements, are not coupled and general solutions can be derived for all k's. Similarly, Eq. (7), referring to the transverse displacements, are not coupled and can be solved analytically within the approximation of *unconstrained-contact*. Full coupling derives from the constraint equations, $w_k = w_{k+1}$, of the *constrained-contact* model that again allows for a closed form general solution.

For the *spring-contact* model, on the other hand, the p's are given by Eq. (6), which results in a system of $m + 1$ coupled differential equations, Eq. (7). Because the springs representing contact do not act in tension, contact may not occur between all of the beam segments intersected by this section. The presence of traction-free crack surfaces simplifies the system of coupled Eq. (7) so that a set of subsystems characterized by a lower number of coupled variables and equations can be defined. The limit cases are those of full coupling of the w_k for $k = 1, \ldots, m + 1$, when contact exists between all segments, and no coupling when all crack surfaces are opened. The coupled differential equations are linear with constant coefficients and the characteristic algebraic equations for the sub-systems can always been found. The general closed form solution of a subsystem composed of one free segment and of 2 or 3 contacting beam segments is shown in Appendix A. A subsystem of more than three beam segments generally requires numerical solution. General solutions of the subsystems for each section of the beam in all possible states of opening and contact can then be determined and used in the iterative procedure to define the regions of contact and opening.

The solution for the whole structure is determined by applying the kinematic and static boundary and continuity conditions to define the constants of integration, C_i, of the general solutions of systems (7) and (8). If the *unconstrained-contact* or the *constrained-contact* model is used, the problem can then be solved in closed form. If the *unconstrained-contact* model predicts no interpenetration between the crack surfaces, the solution is exact. In addition, the regions of crack face interpenetration predicted through the *unconstrained-contact* model give a first approximation of the regions where contact is expected to occur within the *spring-contact* model.

If the *spring-contact* model is used, the regions where crack face contact and opening take place are unknown a priori and must be determined by an iterative solution process. The iterative process is initiated by assuming an initial state of contact along the delamination surfaces. The beam segments formed by the divisions at the crack tips are further subdivided at all coordinates where there is a change in contact state along a delamination surface. At these coordinates, additional continuity conditions are imposed between subdivisions j and k, which correspond to Eqs. (4) with the contributions from beam segment $k + 1$ removed. A system of algebraic equations, corresponding to the boundary and continuity conditions at all divisions of the beam and the general solutions of the governing Eqs. (7) and (8), is constructed based on this assumed state of contact and is solved numerically for the unknown constants of integration, C_i Utilizing the displacement solution, updated regions of delamination surface interpenetration and opening are determined for all delaminations in the system. The updated regions of interpenetration are then assumed to be in contact and a new system of algebraic equations is constructed and solved for the new C_i's. A grid of points is introduced along the axis of each beam segment and the convergence of the solution is checked by considering the norm of the transverse displacements at these locations. The process is repeated until convergence of the solution to a specified tolerance. For all cases examined in this paper, convergence of the solution has been reached easily with only a limited number of iterations.

2.3. Energy release rate and mode decomposition

It is assumed that the n delaminations in the structure are constrained to propagate along the low toughness fracture paths defined by their planes. The energy release rate for the individual coplanar extension of a delamination tip in this system is determined by application of the J-Integral (Rice, 1968) along a

path around the delamination tip. The expression for the J-integral for crack tip i, at the coordinate x_i, separating beam segments j, k and $k+1$ (Fig. 1c), is

$$\mathscr{G}_i = J = \frac{1}{2}\left(\frac{M_k^2}{EI_k} + \frac{N_k^2}{EA_k} + \frac{M_{k+1}^2}{EI_{k+1}} + \frac{N_{k+1}^2}{EA_{k+1}} - \frac{M_j^2}{EI_j} - \frac{N_j^2}{EA_j}\right)\Bigg|_{x_i} \tag{9a}$$

This expression is identical to the expression valid for beams with a single delamination, as is explained in the following. Each crack tip in the beam shown in Fig. 1a can be extracted from the structure as an equivalent beam with a single delamination whose upper and lower surfaces are defined either by the surfaces of the plate or by other delaminations, Fig. 1c. This equivalent single beam is subject to end forces and moments as well as possible contact pressures on its upper and lower surfaces. The path for the J-integral, shown in Fig. 1c, is taken at the crack tip cross sections immediately preceding and following the crack tip and along the upper and lower surfaces of the equivalent beam. For this path, the contact pressures on the upper and lower surfaces do not enter the expression for the J-integral. If there is another delamination tip at the same coordinate x_i the energy release rate is determined as the limit for Δx_i tending to zero of Eq. (9a) applied to a system in which the length of the delamination of interest has been increased (the sign of Δx_i is chosen corresponding to an increase in delamination length) by incrementing the position of the crack tip to $x_i + \Delta x_i$. Expression (9a) is only valid when the rotations of the beams at the crack tips are assumed to be the same, and must be modified accordingly if this assumption is relaxed (see Section 5). Similarly, the equation could be modified to include the contributions due to the shear deformations along the beams.

The above approach cannot be applied to analyze the simultaneous propagation of m delamination tips that have the same coordinate x_m. Instead, the energy release rate in this case is conveniently determined by the variation of the total potential energy with respect to simultaneous unit extension da. The energy release rate for each of the delaminations under this condition is

$$\mathscr{G}_i = \frac{1}{m}\frac{\mathrm{d}W}{\mathrm{d}a}, \tag{9b}$$

where W is the total potential energy of the system. The value of da should be chosen such that it corresponds to an increase in length of the delaminations. For the coordinate system described in Fig. 1, the extension of the left tips of delaminations corresponds to $\mathrm{d}a = -\mathrm{d}x_m$ and the extension of the right tips of the delaminations corresponds to $\mathrm{d}a = \mathrm{d}x_m$. The variation of the total potential energy is also used to analyze the simultaneous propagation of m delamination tips that do not share the same coordinate.

The conditions at the crack tips in the general beam of Fig. 1a are generally mixed mode. The energy release rate calculated using Eqs. (9a) and (9b) includes both the mode I and mode II components, $\mathscr{G}_{\mathrm{I}i}$ and $\mathscr{G}_{\mathrm{II}i}$. Separation of the modes of fracture is accomplished by using the method proposed by Suo (1990), Suo and Hutchinson (1990) and Hutchinson and Suo (1992). They derived analytical expressions for the mixed mode stress intensity factors for a beam with a single crack, with total energy release rate given by Eq. (9a), in terms of the stress resultants, bending moments and normal forces, at the cross sections immediately preceding and following the crack tip, and geometrical parameters. These expressions depend on an additional parameter that can be derived with a rigorous two-dimensional solution of the problem. In the model proposed in this paper, the method is applied to the equivalent beam with a single crack shown in Fig. 1c with energy release rate given by Eq. (9a) and is thus valid for each crack tip in the system.

3. Cantilever beam with *n* equal length delaminations

The first study problem is a cantilever beam of length L with n through width, arbitrarily spaced edge delaminations (Fig. 2) subjected to a static concentrated out of plane force P at its free end. This simple

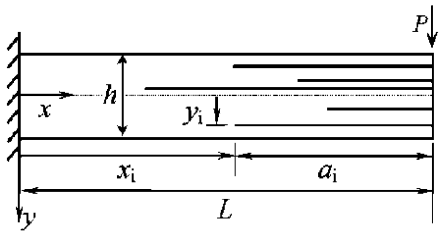

Fig. 2. Cantilever beam with n edge cracks subject to a transverse load P.

structure provides an analytical/semi-analytical description of how multiple delaminations interact. This problem yields results that are identical to those for an edge cracked simply supported beam, loaded by an out of plane force at its mid span. Solutions for simply supported or fixed plates with mid-span, out of plane loading can be simply obtained by modifying the boundary conditions at $x = 0$ and $x = L$. The solution can also be easily extended to circular axisymmetric plates loaded by concentrated out of plane forces at the centers.

In this problem no axial forces are developed; thus the equations governing the axial displacements are ignored. The boundary conditions for this problem are

$$\begin{aligned} &w_0 = 0, \qquad w_{0,x} = 0 \quad \text{at } x = 0, \\ &P = \sum_{k=j}^{j+n} V_k, \qquad M_k = 0, \quad k = j, \ldots, j+n, \\ &w_k = w_{k+1}, \quad k = j, \ldots, j+n-1 \text{ at } x = L, \end{aligned} \tag{10}$$

where j is the index of the uppermost beam segment at the free end of the beam; and as before, the subscripts define the number of the beam segments. Contact of the beam segments under the load point is approximated by assuming that their deflections at the free end are equal. This assumption is exact for the *unconstrained-contact* model and accurate for the *spring-contact* model if the delaminations are long. The static and kinematic continuity conditions at each crack tip are given by Eq. (4).

In the simplest configuration, the delaminations in the beam shown in Fig. 2 are of the same length a. In this configuration, the beam is divided up into $n + 2$ beam segments, $n + 1$ segments forming the cracked region, and one segment forming the uncracked region. Each crack tip is located at the same coordinate $x = L - a$. The continuity conditions (4) are modified as follows:

$$\begin{aligned} &w_0 = w_k, \qquad w_{0,x} = w_{k,x}, \quad k = 1, \ldots, n+1, \\ &M_0 = \sum_{k=1}^{n+1} M_k, \quad V_0 = \sum_{k=1}^{n+1} V_k. \end{aligned} \tag{11}$$

Combining the general solutions for each beam segment for the three contact models allows this system of $4(n + 2)$ boundary and continuity equations to be solved in closed form (Appendix B). The three methods yield identical solutions, which shows that the deflections of the beam segments in the cracked region of the beam are identical and there is no contact or opening along the crack faces.

3.1. Energy release rates for simultaneous propagation of equal length delaminations

The energy release rate for each delamination when the delaminations are assumed to propagate simultaneously is conveniently determined by the variation of the total potential energy W due to a unit propagation of the cracks, Eq. (9b):

$$\mathscr{G}_i = \frac{1}{n}\frac{\mathrm{d}W}{\mathrm{d}a} = \frac{1}{2n}\frac{P^2a^2}{EI_0}\left(I_0 \Big/ \sum_{k=1}^{n+1} I_k - 1\right), \tag{12}$$

where I_0 is the moment of inertia of the intact portion of the beam and I_k is the moment of inertia of the beam segment in the cracked portion of the beam. The next sections will show that for n equally spaced delaminations the energy release rate for simultaneous propagation is higher than the energy release rate corresponding to the propagation of one of the delaminations of the system. On the other hand, when the delaminations are unequally spaced, the response is controlled by the transverse position of the delaminations.

Eq. (12) shows that if the delaminations are uniformly spaced across the entire cross section, then as the number of delaminations increases, the energy release rate per delamination also increases. If on the other hand, the cracks are confined to a band, then as the number of cracks within the band increases the energy release rate per crack decreases. The latter case could represent damage localization in the beam. If a crack growth criterion based on the total energy release rate is applied, the first case would correspond to a decrease of the critical load on increasing the number of cracks, and the second case to an increase of the critical load. However, for the second case, since the cracks are not equally spaced, the assumption of simultaneous propagation may not be valid and the critical load could be defined by the propagation of only one of the cracks of the system.

3.2. Stability of the equality of length in a system of equal length delaminations

The equality of length will be said to be stable in a system of equal length delaminations if the system recovers the condition of equal length after the lengths of one or more cracks are perturbed.[1] It will be shown later that, for a fixed number of delaminations, the energy absorption is higher if the equality of length is stable than if it is not.

3.2.1. Equally spaced delaminations

This special case was previously examined by Suemasu and Majima (1996) who investigated the stability of the equality of length of an axisymmetric system of equally spaced, penny-shaped delaminations in a clamped circular plate subject to a concentrated out-of-plane load. The study was performed under the simplifying kinematic assumption of *constrained-contact*. This assumption is relaxed here, and the stability of the equality of length is studied using the *spring-contact* model. The problem is greatly simplified by noting that in the limit of the delaminations having the same length, the solution of the *spring-contact* model is identical to that of the *unconstrained-contact* model. Closed form solutions can therefore be found, which are detailed in Appendix C and summarized below.

An ideal system of equal length, equally spaced delaminations propagates when the energy release rate, given by Eq. (12), equals the fracture energy of the material. If a positive perturbation of the length of crack i in the system is considered, then the energy release rate for the propagation of that crack is lower than that corresponding to the simultaneous propagation of the remaining cracks. Thus, using a fracture criterion based on the total energy release rate, the remaining delaminations will grow up to the length of the perturbed delamination and equality of length will be restored. Conversely, if a negative perturbation of the length of crack i is considered, then the energy release rate of crack i is higher that of the remaining cracks: the system is again stable. Since a negative perturbation of one crack is identical to a positive perturbation

[1] The term stability is used here to refer to changes in the crack geometry and *not* the question of whether the crack growth is quasi-static (stable) or dynamic (unstable).

of the remaining cracks and vice versa, conclusions on the effect of positive or negative perturbations of one crack will also hold for perturbations of a generic number of cracks.

The same conclusions are reached if the simplifying kinematic assumption of *constrained contact* is used. The analysis, which is similar to that presented in the Appendix C, is not presented here. Suemasu and Majima (1996) obtained the same results for axisymmetric clamped circular plates.

3.2.2. Unequally spaced delaminations

A system of unequally spaced, equal length delaminations does not always grow self-similarly, even in the absence of length perturbations. The question of stability of the equality of length is controlled by the through-thickness position of the delaminations. The map of Fig. 3 refers to a two-crack system and has been constructed by using the *spring-contact* model. Similar results are obtained using the *unconstrained-contact* model. Fig. 3 shows regions in which the energy release rates for the propagation of one of the two cracks, $\mathcal{G}_U$ and $\mathcal{G}_L$, and for their simultaneous propagation, $\mathcal{G}_B$, have different ordering. The map is a function of the through-thickness positions of the two cracks. The upper crack is located at a distance h_3 from the upper surface of the beam and the lower crack is located at a distance h_5 from the lower surface of the beam, as shown in the inset in the figure.

The map shows three regions: region I in which $\mathcal{G}_U > \max(\mathcal{G}_L, \mathcal{G}_B)$; region II in which $\mathcal{G}_B > \max(\mathcal{G}_U, \mathcal{G}_L)$; and region III in which $\mathcal{G}_L > \max(\mathcal{G}_U, \mathcal{G}_B)$. Thus in regions I and III, only one crack will propagate when critical conditions are satisfied, while in region II, both cracks propagate together. Furthermore, in regions I and III, the system is more unstable (increasing difference between the highest and next highest values of $\mathcal{G}_U$, $\mathcal{G}_L$, and $\mathcal{G}_B$) under positive perturbations of the length of the upper crack (region I) and to negative perturbations of the length of the lower crack (region III).

For cases lying in region II the system is stable to both positive and negative perturbations. Thus, in this region the delaminations will always grow self-similarly. The solution of equally spaced delaminations is represented in the diagram by a point in the shaded pocket at $h_3 = h_5 = 1/3h$.

In the case of unequally spaced delaminations, the *constrained-contact* model yields a map with a larger region of stability than that shown in Fig. 3. The region is shown in Fig. D.1b. This difference highlights the limitations of the simplified contact models when applied to general delamination geometries.

In a real structure, the location of the delaminations through the thickness of the plate will depend on the internal structure of the material and the loading conditions, which therefore determine the conditions for the stability of the equality of length of the system.

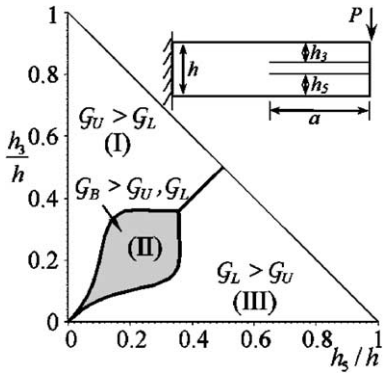

Fig. 3. Map of regions of different energy release rate for a system with two cracks.

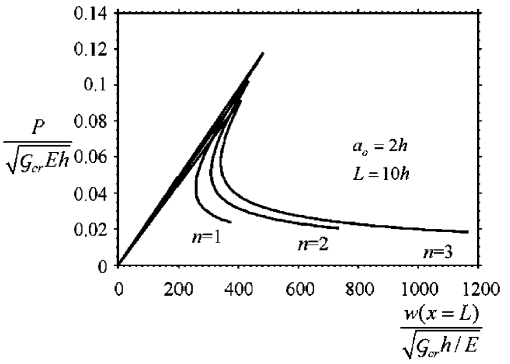

Fig. 4. Dimensionless diagram of the critical load for crack propagation versus load–point displacement for a cantilever beam of n equal length and equally spaced cracks.

3.3. Macrostructural response

The macrostructural behavior of a plate of length $10h$ with n equally spaced delaminations, $h_k = h/(n+1)$, of equal initial length $a_0 = 2h$ is shown in Fig. 4. The delaminations have been assumed to propagate when $\mathcal{G}_i = \mathcal{G}_{cr}$, where $\mathcal{G}_{cr}$ is the fracture energy of the material. The figure shows the normalized critical load for the propagation of the crack system as a function of the normalized load point displacement. As the number of delaminations increases, the critical load for initial growth of the delaminations decreases and the post-peak behavior of the structure becomes more ductile. This is to be expected as diffuse damage leads to a more ductile structural response and increased energy absorption. In contrast, localized damage, for instance the propagation of a single crack, results in an increased ultimate capacity of the structure, but in a less ductile response and decreased energy absorption.

4. Cantilever beam with two unequal length delaminations

In a general system of delaminations with unequal length and spacing, Eq. (12) and the conclusions and results of the previous section do not apply and the general problem defined by Eq. (7) must be solved in order to define energy release rates. In this section, a system of only two cracks is studied, in which many of the characteristics expected of general cases can be observed, without distracting complexity. In most cases, the behavior of the system depends on only three dependent variables, allowing complete visualization of the interaction effects.

A cantilever beam of length L and height h with two edge delaminations of arbitrary length and spacing is shown in Fig. 5. The length of the upper delamination is a_U and the length of the lower delamination is a_L. The through-thickness positions of the delaminations are defined by h_3 and h_5, where h_3 is the distance of the upper delaminations from the upper surface of the beam and h_5 is the distance of the lower delamination from the lower surface of the beam. Utilizing the three approximations for treating contact, the system of equations formed by the boundary conditions Eqs. (10) and continuity conditions Eqs. (4) together with Eq. (7) has been solved for the three possible configurations of the system, $a_U = a_L$ (Section 3), $a_U > a_L$ (Fig. 5a) and $a_U < a_L$ (Fig. 5b).

4.1. Energy release rate

Solutions for the energy release rate of the different configurations of the system are presented in Appendix D. Appendix A also presents in Fig. D.1 maps constructed for a general through-thickness distribution

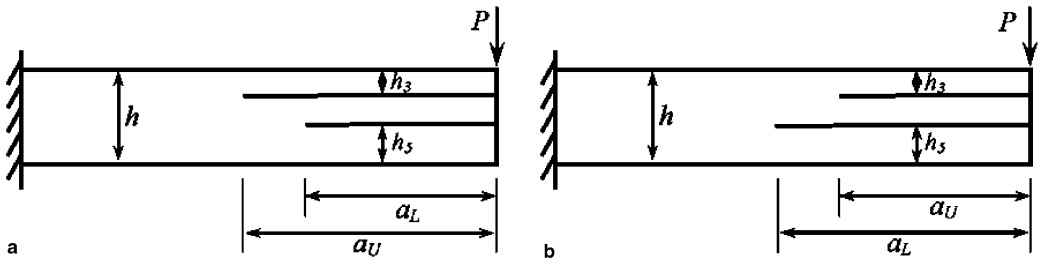

Fig. 5. Cantilever beam with two arbitrarily spaced cracks.

and lengths of the delaminations that show regions in which the energy release rate of one of the cracks is higher or lower than that of the other crack and can be used to analyze crack propagation in the system.

Fig. 6 shows exemplary solutions for a system of two equally spaced cracks ($h_3 = h_5 = h/3$). Fig. 6a defines the energy release rate of the upper crack on varying its length, while the length of the lower crack is kept fixed at $a_L/h = 5.0$. Fig. 6b defines the energy release rate of the lower crack on varying its length, while the length of the upper crack is kept fixed at $a_U/h = 5.0$. The figures show a comparison of the energy release rates calculated using the three approximations of contact (solid curve = *spring-contact*, dashed curve = *unconstrained-contact* and dash-dot curve = *constrained-contact*). Numerical results from these figures and others show that the *unconstrained*-and *constrained-contact* models define upper and lower bounds of the *spring-contact* model for all through-thickness distributions of the cracks. Fig. 6 also shows by the

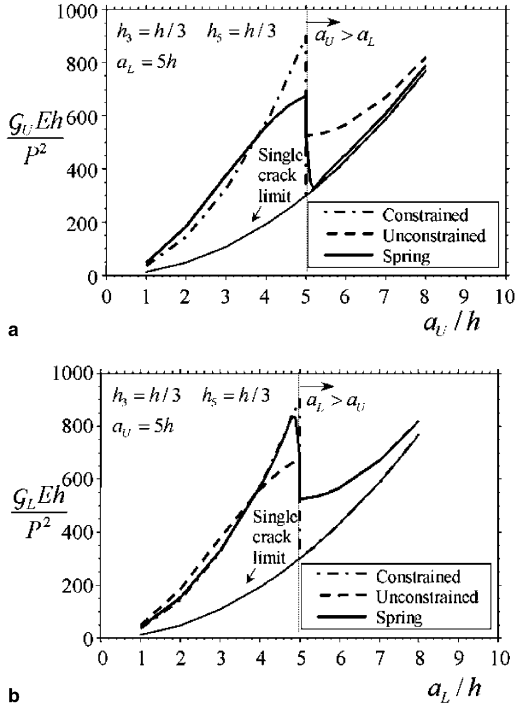

Fig. 6. Normalized energy release rates of two equally spaced cracks in the beam of Fig. 5 as a function of the length of the cracks. (a) Upper crack, (b) lower crack.

thin line the energy release rate of the crack in the absence of the other crack, or the single crack limit. The limit is approached when the interaction effects disappear. The *constrained-contact* model reaches this limit immediately after the discontinuity in energy release rate. Zheng and Sun (1998) showed similar behavior for the longer delamination of two central, through-width delaminations in a three-point bending specimen.

Fig. 6a and b show that in the equally spaced delamination system studied there is a strong interaction effect on the energy release rate, which is always amplified with respect to the single crack solution. The next section will show that different solutions, characterized by shielding, amplification or a combination of both, are found for other crack systems. In addition seems out of place reach the same length there are negative discontinuities of the same magnitude in their energy release rates. It will be shown in Section 5 that the discontinuity is a good approximation of a sharp change in energy release rate shown by a full numerical solution of the problem. In other material systems a similar behavior has been observed. For instance, from the 2-D solution of an infinite body with a main crack interacting with ordered arrays of micro-cracks, sharp jumps in the stress intensity factors have been noted as the main crack tip moves through the array (Brencich and Carpinteri, 1996).

4.2. Shielding and amplification of the energy release rate

As observed in the previous section, a delamination in a system of delaminations can either amplify or shield the energy release rates of the other delaminations or have no influence on them. This effect can be synthesized for the crack system of Fig. 5 by considering diagrams of the energy release rate of a crack, $\mathcal{G}_i$, normalized with respect to the energy release rate of the same crack when the other crack is not present, $\mathcal{G}_{io}$.

The energy release rate of a crack is always amplified by the presence of a shorter crack independent of their through-thickness positions, which only affect the magnitude of the amplification (the *constrained-contact* model erroneously predicts for this regime neither amplification or shielding). A longer crack can have different effects on a shorter crack, with the sense of the effect depending on their through-thickness positions and, in some regimes, their lengths. The maps shown in Fig. 7a and b have been obtained using the *spring-contact* model (identical results are obtained assuming *unconstrained-contact*). The dashed lines in the figures are solutions of the *constrained-contact* model.

If the point describing the positions of the two delaminations falls in the upper region (III), the shorter delamination will always be shielded by the longer. The magnitude of the shielding effect depends on their

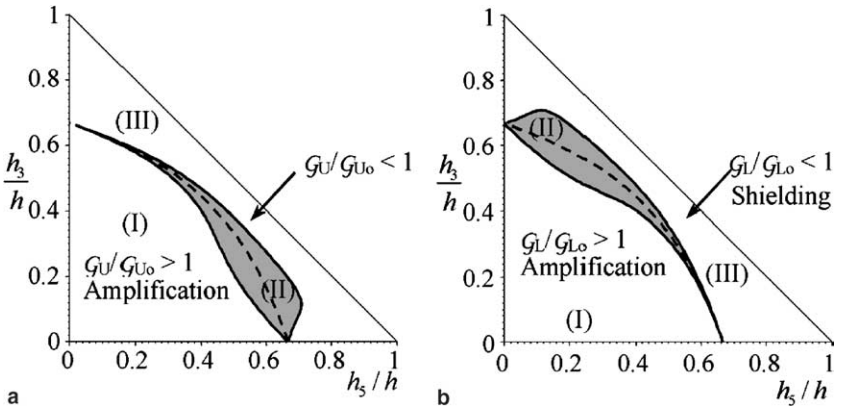

Fig. 7. Map of shielding and amplification of the energy release rate for a crack in the presence of a longer crack (schematic of Fig. 5). Shaded regions (II) indicate a combination of shielding and amplification depending on the length of the delaminations. (a) Upper crack, (b) lower crack.

lengths. If the point falls in the lower region (I), the energy release rate of the shorter delamination will always be amplified by the longer. If the point falls in the middle region (II), either amplification or shielding can occur for the shorter crack, depending on the two lengths. The solution of the *constrained-contact* model does not have a region of mixed shielding and amplification. The dashed line in Fig. 7 corresponds to crack configurations where $\mathcal{G}_{\mathrm{L}} = \mathcal{G}_{\mathrm{L0}}$ and separates regions of shielding (III) and amplification (I). This simplified model is unable to predict the complex details of multiply delaminated systems.

An example considering the energy release rate of the lower delamination for a through-thickness position of the cracks that falls in region (I), showing amplification of $\mathcal{G}_{\mathrm{L}}$, is presented in Fig. 8a. The figure shows $\mathcal{G}_{\mathrm{L}}$ normalized with respect to $\mathcal{G}_{\mathrm{L0}}$ on varying a_{L} with the length of the upper crack fixed at $a_{\mathrm{U}}/h = 5.0$. When the lower crack is shorter than the upper crack, there is a strong amplification of $\mathcal{G}_{\mathrm{L}}$ with

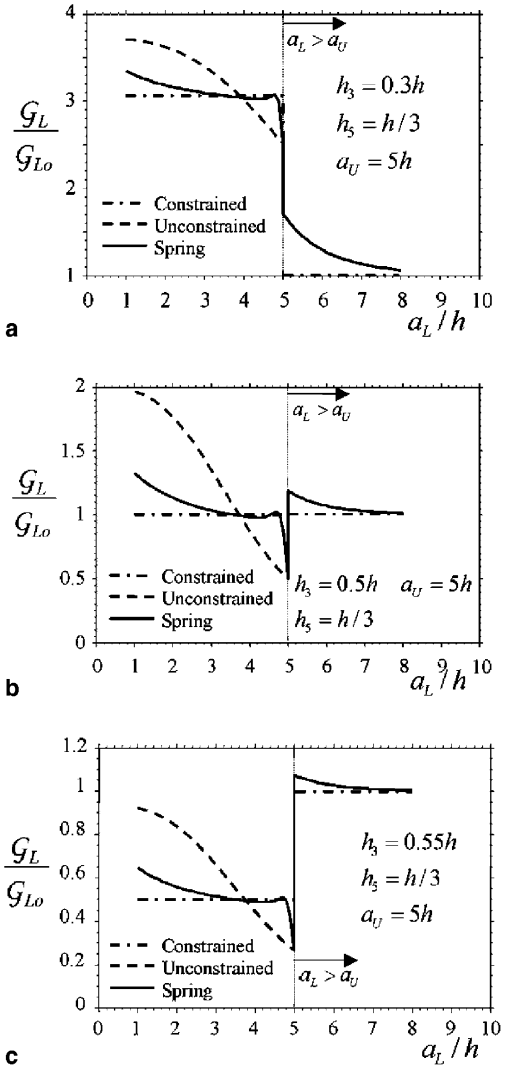

Fig. 8. Examples of shielding and amplification of the energy release rate of the lower crack in the two-crack system of Fig. 5 (upper crack length fixed).

an amplification factor around 3. The amplification is then reduced by the discontinuity (localized shielding effect), when the two cracks have the same length, and it decreases on increasing the length of the crack. An example of shielding of $\mathcal{G}_L$, a point in region (III), is shown in Fig. 8c. In this case the discontinuity in $\mathcal{G}$ corresponds to a localized amplification effect. An example of both shielding and amplification depending on the lengths of the delaminations, a point in region (II), is shown in Fig. 8b.

In this structure the shielding of one of the delaminations is always accompanied by the amplification of the other delamination. Among all the possible through-thickness distributions and lengths of the delaminations, the effect of the interaction can be very strong, and it has been verified numerically that the energy release rate can be amplified up to 600% by the presence of a much longer delamination.

Brencich and Carpinteri (1996) showed qualitatively similar amplification and shielding effects when considering the interactions of a main crack propagating through a pair of symmetrically located microcracks in an infinite body. For this problem the magnitude of the shielding and amplification depends on the spacing between the cracks, but the qualitative behavior of the shielding and amplification is unaffected by this distance. In contrast, for the structural delaminations discussed in this paper, due to geometrical effects, the through-thickness position of the delamination may alter the condition of shielding or amplification, not just their magnitudes. This is in agreement with the numerical study of the interaction of two central delaminations in a three-point bending specimen of Zheng and Sun (1998).

4.3. Mode ratio

Mode decomposition has been performed for the exemplary system of two equally spaced delaminations. Fig. 9 shows the relative amount of mode II to mode I defined by the phase angle $\Psi = \tan^{-1}(K_{II}/K_I)$. Fig. 9a defines Ψ_U for the upper delamination on varying its length, while the length of the lower delamination

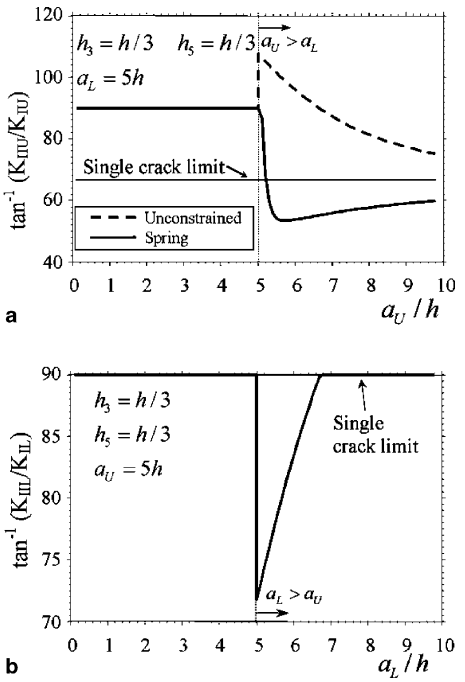

Fig. 9. Relative amount of mode II to mode I stress intensity factors in the two-crack system of Fig. 5.

is kept fixed at $a_L/h = 5.0$. Fig. 9b defines Ψ_L for the lower delamination on varying its length, while the length of the upper delamination is kept fixed at $a_U/h = 5.0$.

The figures compare solutions obtained using the *spring-contact* model (thick solid line) with the *unconstrained-contact* model (dashed line) and the solution of a single delamination Ψ_0, in the absence of the other delamination (thin line). For a single delamination, the relative amount of mode II to mode I is independent of the delamination length and given by $\Psi_{U0} = 66.7°$ for the upper delamination and by $\Psi_{L0} = 90°$ for the lower delamination (the lower delamination experiences pure mode II conditions due to localized contact at the crack tip).

Fig. 9a shows that when the upper delamination is shorter than the lower, the conditions are pure mode II. Comparison with the single delamination solution highlights the strong effect produced by the presence of the lower delamination. When the upper delamination reaches the length of the lower delamination there is a sharp transition and the mode I component is suddenly increased above the corresponding single delamination solution (thin line). As the upper crack lengthens, the interaction decreases and the solution tends to the single delamination limit. The dashed curve highlights the limitations of the simplified *unconstrained-contact* model, which predicts an unrealistic phase angle $\Psi > 90°$, due to the interpenetration of the delamination surfaces.

Fig. 9b shows that the lower delamination is in pure mode II conditions due to contact at the delamination tip when its length is shorter than the length of the upper delamination and this solution coincides with the solution of the single delamination. When the lower delamination approaches the length of the upper delamination, there is a sudden transition (solid curve) to a large value of the mode I component. The interaction effect then disappears quickly as the lower delamination lengthens and the solution tends again to the solution of a single delamination. Interestingly, when the lower delamination is longer, the bending theory model always predicts opening at the lower delamination tip even when the mode decomposition method defines a negative mode I stress intensity factor and therefore pure mode II conditions (shown in Fig. 9b for $a_L/h > 6.75$). This fictitious opening displacement field is a consequence of neglecting the root rotations at the delamination tip, which if properly accounted for would restore contact (Andrews et al., 2005).

4.4. Delamination growth and macro-structural behavior

To investigate the macro-structural response of the plate, the quasi-static propagation of the system of two delaminations shown in Fig. 5 has been studied using the *spring-contact* model. A delamination has been assumed to propagate when its energy release rate equals the fracture energy of the material, $\mathcal{G}_{cr}$. The cracks have been assumed to grow under delamination length control, which allows virtual delamination growth branches to be followed. Several cases, identified by different through-thickness positions of the delaminations and different notch lengths as shown in Figs. 10–13, have been considered to highlight a number of interesting macrostructural responses of the system. The figures show the critical load for crack propagation as a function of the load point deflection. Also shown in the inset in the figures is the evolution of the lengths of the delaminations; the dashed line shows the length of the lower delamination and the solid line shows the length of the upper delamination during the loading process.

For the first delamination configuration, shown in Fig. 10, the lower delamination starts to propagate first at (A). The propagation is unstable up to point (B), where the delamination reaches the upper delamination. At this point the delamination arrests and the delamination system can be made to propagate only by increasing the applied load. This behavior is due to a negative discontinuity, shielding, in the energy release rate. After point (C) the lower delamination continues to propagate unstably until the structure fails. A snap-back instability is present as the lower delamination grows to the upper delamination.

In the case shown in Fig. 11 the lower delamination begins to propagate unstably at point (A). At (B) the delaminations are of the same length and there is a sudden drop in the critical load, corresponding to a

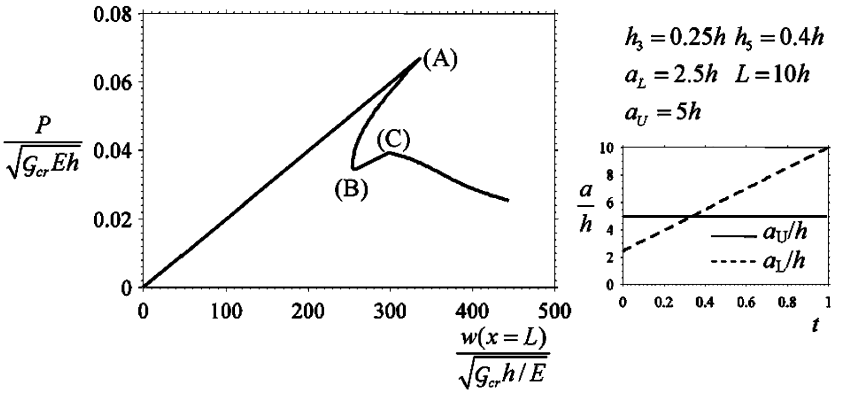

Fig. 10. Dimensionless diagram of the critical load for crack propagation versus load–point displacement in the two-crack system of Fig. 5: snap-back instability and local increase in critical load due to a local shielding effect.

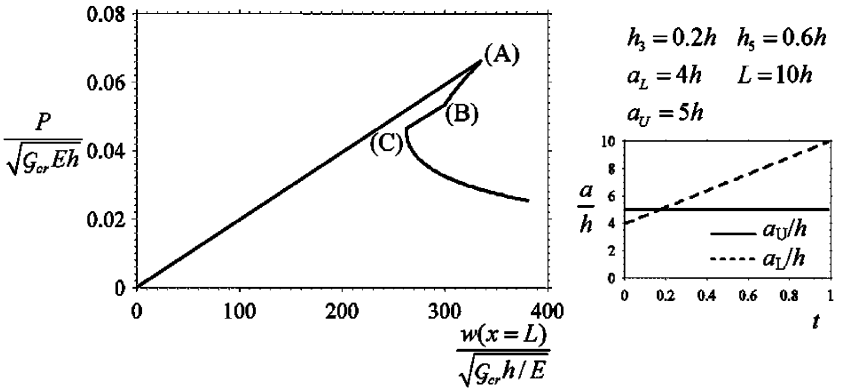

Fig. 11. Dimensionless diagram of the critical load for crack propagation versus load–point displacement in the two-crack system of Fig. 5: snap-back instability with local drop in critical load due to a local amplification effect.

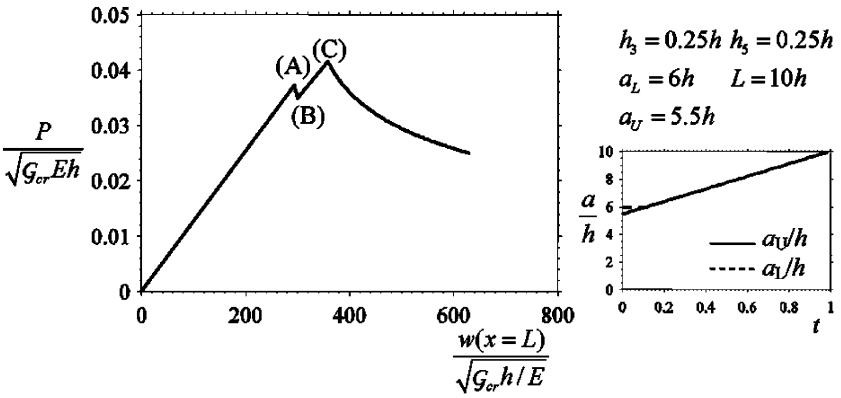

Fig. 12. Dimensionless diagram of the critical load for crack propagation versus load–point displacement in the two-crack system of Fig. 5: snap-through instability and hyper-strength phenomenon due to a local shielding effect.

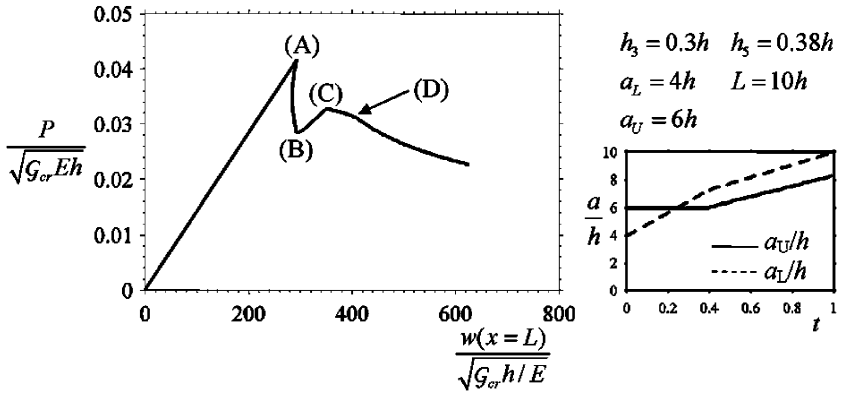

Fig. 13. Dimensionless diagram of the critical load for crack propagation versus load–point displacement in the two-crack system of Fig. 5: crack pull along.

positive discontinuity, amplification, of the energy release rate. The lower delamination then continues to propagate unstably.

The case shown in Fig. 12 is similar to that examined in Fig. 10. However in this case the new critical load due to the negative discontinuity, shielding, in the energy release rate is higher than the initial load for delamination propagation. This is an interesting example of hyperstrength, which is defined as the condition that the ultimate load of the structure exceeds the load corresponding to the first propagation of one of the delaminations of the system even in the absence of any strengthening mechanisms. The hyperstrength is produced by the elastic interactions of the parallel delaminations that create local shielding and hardening effects, leading to a snap-through instability.

An example of crack pull-along, in which the finite propagation of one delamination causes the propagation of the other delamination, is shown in Fig. 13. In this case the lower delamination propagates first at point (A). When it reaches the second delamination at point (B), there is an increase in critical load due to a negative discontinuity in energy release rate. The lower delamination continues to propagate at point (C). At point (D), the upper delamination begins to propagate, and both delaminations continue to propagate, keeping a constant relative length until the structure fails. This behavior occurs for through-thickness distributions of the delaminations that fall just to the right or just above the shaded region of the map of Fig. D.1a, and just to the right of the shaded region in the map of Fig. D.1b.

5. Validation of the proposed model

The proposed model, applied to the problem of a cantilever beam with two edge cracks, has been validated using the finite element method (FEM) and the commercial code ANSYS (5.5). The mesh consisted of plane stress isoparametric triangular elements. To obtain an accurate solution, including relative crack displacements, while keeping the number of degrees of freedom low, a coarse mesh was used for the body of the beam and very fine meshes around each crack tip and along areas of contact. The stress singularities at the crack tips were modeled with rosettes of quarter point elements. Contact along the crack faces was simulated using gap elements that prevent interpenetration of the beams with stiff linear springs. Convergence of the solution was checked by varying the size and number of elements and stiffnesses of the gap springs. Energy release rates were calculated by two methods, the J-Integral, Rice (1968), and the displacement correlation method, Chan et al. (1970), which was also used to evaluate the mode ratio. The path of the J-integral was chosen within a fine mesh region so that it encompassed sufficient elements for its value to converge.

5.1. Comparison of energy release rates

The energy release rates determined by the finite element method and the present *spring-contact* model are shown in Fig. 14a for a system of two equally spaced cracks ($h_3 = h_5 = h/3$). The error between the two solutions is shown in Fig. 14b. In the figure, the normalized energy release rate of the upper crack is depicted as a function of the length of the upper crack. The length of the lower crack is kept fixed at $a_L/h = 5.0$.

Fig. 14a and b show that the results of the proposed model generally agree with the finite element results. When the cracks reach the same length, the finite element solution predicts a continuous transition in energy release rate. This transition matches the discontinuity in energy release rate predicted by the beam theory model.

Short cracks ($a_U < 2h$ for the geometry of Fig. 14) are characterized by large errors due to the well-known limitations of classical beam theory. As expected, the error drops when the length of the crack increases, provided it is not similar to the length of the other crack, to less than 5% when $2h < a_U < 4.6h$ or $a_U > 7.0h$. Where the two cracks have similar lengths and the energy release rate is characterized by a discontinuity, the error increases significantly (up to 30% for the geometry studied in Fig. 14). The width of this region is given by a few times the separation of the planes of the interacting cracks and depends on the conditions of the crack surfaces (contact or opening). For the geometry studied in Fig. 14, the error is above 5% for $4.6h < a_U < 7.0h$. The interval is not symmetric about the length of the lower crack, $a_L = 5h$, because of the different conditions along the crack surfaces when the upper crack is shorter (opening) or longer (contact) than the lower. Numerical calculations show that behaviors similar to that observed in Fig. 14 characterize all possible crack configurations and that the width of the region where the error increases significantly is always a few times the distance between the planes of the cracks.

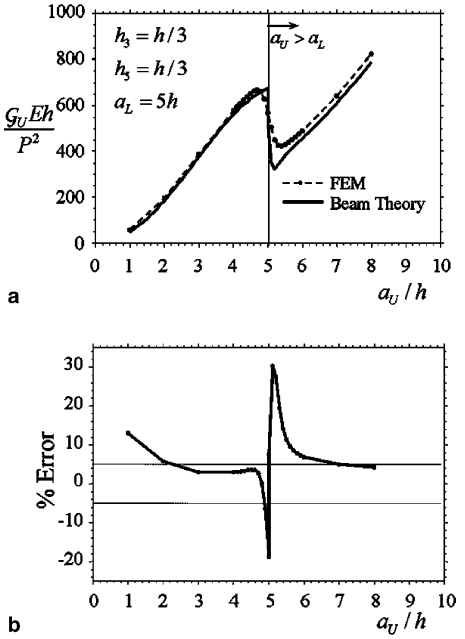

Fig. 14. (a) Energy release rate of the upper crack in the two-crack system of Fig. 5: comparison between FE and proposed model results. (b) Relative error between the solutions of (a) (dashed line indicates a 5% relative error).

5.2. Comparison of mode ratios

The relative amount of mode II to mode I as measured by the phase angle $\Psi = \tan^{-1}(K_{II}/K_I)$ determined by the finite element method and the model presented in this paper utilizing the *spring-contact* approximation is shown in Fig. 15. Fig. 15a shows the phase angle of the upper crack as a function of the length of the upper crack, while keeping the length of the lower crack fixed at $a_L/h = 5.0$. Fig. 15b shows the phase angle of the lower crack while keeping the length of the upper crack fixed at $a_U/h = 5.0$.

The phase angles of the lower crack determined by the two models, shown in Fig. 15b, agree well with the relative error peaking near the discontinuity at only 10%. Fig. 15a instead shows a significant difference, with an error up to 26%, between the results of the bending theory model and FEM when the upper crack is longer and there is contact along both delamination surfaces. When the lower crack is longer and there is no contact along the delamination surfaces, the error is instead very low. This result confirms what has already been observed for the energy release rate. However, the width of the region where the relative error on the mode ratio is quite large and is greater than that corresponding to the energy release rate.

5.3. Discussion

The relative error between the model and the FE predictions, as observed in Figs. 14 and 15, is greater when there is contact between the crack surfaces. This is mainly due to the assumption of the proposed model of zero relative root rotations of the sublaminates at the crack tips that leads to an overestimation of the contact pressures. The effects of the root rotations on the contact pressures and thus on the energy release rate and mode ratio are most significant when the cracks are close to the same length $|a_U - a_L| < h$ and are stronger on the mode ratio. When there is no contact along the crack faces, neglecting the root

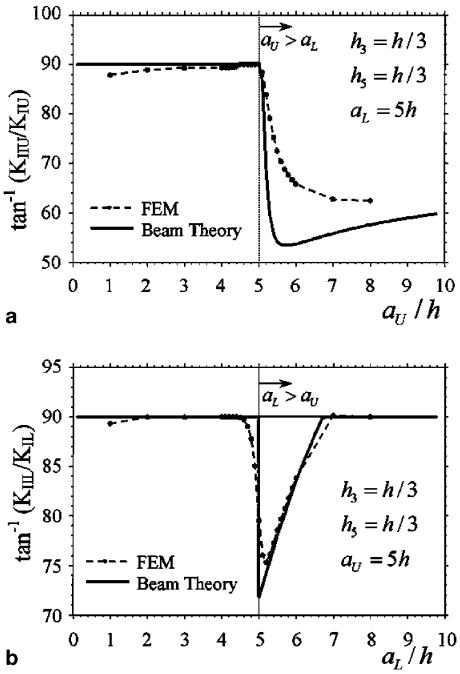

Fig. 15. Relative amount of mode II to mode I for a two-crack system: comparison between proposed model and FE results.

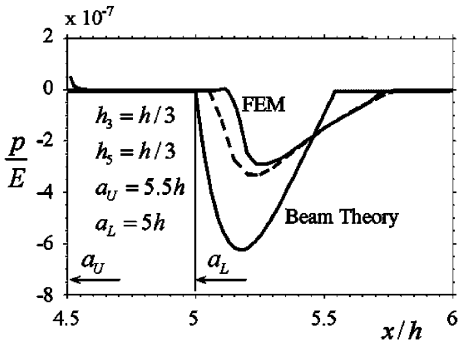

Fig. 16. Comparison of predicted contact pressures along the faces of the upper crack in the two-crack system (dashed line: contact pressures using the FE displacement field and *spring-contact* approximation).

rotations does not significantly affect the solution, confirming what has already been observed for single delaminations loaded primarily in shear.

The contact pressure distribution along the surfaces of the upper crack, for equally spaced cracks with lengths $a_U/h = 5.5$ and $a_L/h = 5$, predicted by the proposed model and the FE method are shown in Fig. 16 as a function of the position along the crack. The model predicts a peak pressure double that of the FE solution. These discrepancies in the solutions cannot be attributed to the contact approximation used in the model: using the centerline beam deflections obtained in the FE solution and Eq. (6) to predict the contact pressure leads to the pressures identified by the dashed curve that for magnitude and shape closely follow the finite element solution. Including shear deformations in the model improves the pressure distribution, but does not substantially improve the values of the energy release rate.

The overestimation of the contact pressures is associated with significant errors in the stress resultants at the crack tip. This is shown in Table 1 where bending moment and shear force obtained using the proposed model are compared with the FE results (rows 2 and 1). Table 1 also compares the energy release rates and phase angles obtained using the proposed model (row 2) and the FEM (row 1) and highlights the previously noted large errors. If the actual FE stress resultants are used instead of the model resultants in Eq. (9a) and in the expressions of Suo and Hutchinson for the stress intensity factors, the solution is still affected by large errors. This is shown in row 3 of the table. The reason for this discrepancy is that both Eq. (9a) for the energy release rate and Suo and Hutchinson's expressions do not account for the contributions due to the shear deformations along the beams and the deformations at the crack tip cross sections (i.e., root rotations).

The expression (9a) for the energy release rate can be modified to account for these effects as follows:

$$\mathscr{G}_i = J = \frac{1}{2}\left(\sum_{l=k}^{k+1}\left(\frac{M_l^2}{EI_l}+\frac{V_l^2}{\kappa GA_l}+\frac{N_l^2}{EA_l}-2V_l\varphi_l\right)-\frac{M_j^2}{EI_j}-\frac{V_j^2}{\kappa GA_j}-\frac{N_j^2}{EA_j}+2V_j\varphi_j\right)\Bigg|_{x_i}, \tag{13}$$

where $\mathscr{G}$ is the shear modulus, κ is the shear correction coefficient (5/6 for a rectangular cross section), V and φ are the shear resultant and the bending rotation respectively.

Li et al. (2004) recently modified the stress intensity factor expressions derived by Suo and Hutchinson to include the contributions of the shear deformations along the beam and the crack tip deformations numerically. Wang and Qiao (2004) proposed an analytical extension of the method of Suo and Hutchinson. Rows (4) and (5) in the Table show solutions obtained using these two methods. Both methods lead to substantial improvement in the solutions. The method of Wand and Qiao relies on the assumptions of plate theory in order to determine the crack tip rotations, and thus is not as accurate as the numerical solution of Li et al.

Table 1
Stress resultants, energy release rate and phase angle of the upper crack

		Moment—upper beam arm (M/Ph)	Moment—lower beam arm (M/Ph)	Shear—upper beam arm (V/P)	Shear—lower beam arm (V/P)	Ψ_U, % Error from FEM	$\mathcal{G}_U Eh/P^2$, % Error from FEM
(1)	FE stress resultants $\mathcal{G}$ and Ψ Displacement correlation Technique	−0.967	−4.535	−0.644	1.644	72.4°	428.59
(2)	Proposed model	−0.300	−5.200	−1.752	2.752	54.2°, 25.18%	380.89, 11.13%
(3)	FE stress resultants $\mathcal{G}$ Eq. (9a) Ψ after Suo and Hutchinson	−0.967	−4.535	−0.644	1.644	80.9°, −11.66%	386.14, 9.91%
(4)	FE stress resultants $\mathcal{G}$, Ψ after Li and Thouless	−0.967	−4.535	−0.644	1.644	72.2°, 0.31%	430.18, −0.37%
(5)	FE stress resultants $\mathcal{G}$ Eq. (13) Ψ after Wang and Qiao	−0.967	−4.535	−0.644	1.644	74.4°, −2.71%	417.65, 2.55%

Equally spaced cracks, $a_U/h = 5.5$, $a_L/h = 5$, $h/L = 0.1$.

The observations above highlight that the model proposed in this paper could be improved substantially by: removing the assumption of zero relative root rotations at the crack tips, for instance by using localized linear elastic rotational springs (Pandey and Sun, 1996); including the contribution of shear deformations along the beams; applying Eq. (13) for the energy release rate and an extended solution, e.g. of Li et al. (2004) or Wang and Qiao (2004), for the decomposition of the modes of fracture. This would lead to a more accurate quantitative prediction of the displacement fields along the crack surfaces and the fracture parameters of the system. Such an approach would become necessary, and would probably be sufficient for plane conditions, if the influence of crack-wake mechanisms, such as bridging or cohesive mechanisms and friction, on the fracture behavior of multiply delaminated plates is to be investigated.

6. Application of the proposed model to the design

6.1. Beam theory for quantitative analyses

Elastic analyses of laminates that are based on plate elements are widely used and accurate for many design predictions. Extended laminar sheets comprising thin plies do indeed very nearly satisfy the conditions of strain distribution necessary for the reduced degrees of freedom in beam (or plate) theory to be sufficient.

As shown in this paper, modeling delamination fracture is, however, much more challenging. In multiply delaminated beams as well as other more complex structures, delaminations propagate in mixed mode, often predominantly in shear (modes II and III). Crack propagation, even in the absence of a through-thickness reinforcement (stitching, pins, etc.), will therefore be very strongly and commonly influenced by contact forces and crack face friction. Other crack wake effects, such as bridging by fibers or craze fibrils, might also be important. The tractions imposed on the fracture surfaces by such effects will depend, possibly sensitively, on the mixed mode crack displacement vector; and therefore accurate prediction of the crack displacement becomes a prerequisite to a full quantitative model of delamination.

The question of whether plate or beam theory methods can deal with quantitative delamination analysis turns on the success of estimates of root rotations, which control the accuracy of crack displacement predictions near crack tips. Our current work and work in the literature (Andrews et al., 2005; Sun and Pandey, 1994; Pandey and Sun, 1996) encourages the view that reasonably simple root rotation corrections can indeed restore accuracy. If so, beam theory may be not only useful but even the preferred method, especially for plane problems, including many common experimental tests, since it yields straightforward, relatively small numerical problems and, in many important cases and limits, highly instructive analytical results.

Competition in accurate delamination modeling will come from modern cohesive element methods, which are extensions of finite element formulations to include elements that can introduce bridging and contact tractions in convenient ways. Cohesive models are an attractive, physically based formulation of nonlinear crack tip and crack wake processes, very well suited to complex 3D configurations with arbitrary mode mixtures. They have a growing record of successful simulations of experiments (e.g., Remmers et al., 2003; Yang and Cox, 2004). However, accurate cohesive model analyses of complex laminated structures may comprise 10^6 degrees of freedom and do not yield analytical results, even in limits. Beam theory and computationally intensive cohesive element methods may prove complementary.

6.2. Towards structural design concepts

Many configurations of loads and boundary conditions arise in structures other than the cantilever case studied here. Nevertheless, the cantilever case suggests some principles concerning the role of the multiplicity of delaminations in structural performance that may prove generally applicable to cases of mixed shear and bending.

Assume that residual strength following delamination damage declines as the size of the cracks increases (e.g. Fig. 4). Then the results for uniformly spaced cracks (Eq. (12)) suggest that, to enhance residual strength, material conditions that favour greater number of cracks uniformly distributed through a structure are to be avoided. On the other hand, if the cracks are confined to a band of limited width, then resistance to growth *rises* with their number. Protection against long cracks might therefore be sought by deliberately introducing multiple weaker planes within a limited band in the material. Of course, the effect of such a strategy on other failure routes must also be considered. For instance by tailoring the material for increased residual strength the ductility of the structure is reduced, leading to a more brittle failure of the structure.

The case study of the system of two cracks shows that interaction effects are strong. Cases in which one crack shields the other and cases in which it leads to accelerated growth in its partner can be found, depending on where the two cracks reside in the laminate. The possibility of acceleration implies that design and life predictions based on solutions for a single crack cannot be safe.

In many cases studied here, the possibility of crack face contact arises. Long zones of crack wake contact and friction can therefore be expected to be common in structural problems involving shear and bending. The friction zones will not generally be confined to a near-tip region, in particular one that is sufficiently small that friction effects could be incorporated by modifying the critical value of the energy release rate. Rather, the friction contact zone will vary in extent (and possibly in the number of contact domains) with the crack size and its relation to other cracks. The contact zones must be calculated explicitly. Similar remarks will apply to treating through-thickness reinforcement, should it be present. Work is in progress to investigate these topics.

7. Conclusions

A model has been presented that allows for the analysis of laminated plates with multiple delaminations deforming in cylindrical bending. The model utilizes the assumptions of classical beam theory, which

neglects shear and near-tip deformation, and accounts for non-frictional contact between the crack surfaces. It has been applied to a cantilever beam with multiple through-width edge delaminations subject to a concentrated load at its free end. Contact has been simulated using different approaches, *unconstrained-*, *constrained-* and *spring-contact*, where the names reflect the approximation used to describe the displacement field. Finite element analyses applied to a two delamination system show that the *spring-contact* model is the most accurate; however utilizing it results in a non-linear problem and thus requires a partially numeric solution while the other models result in closed form solutions. The two simpler approximations give upper and lower bounds of the energy release rate determined by the *spring-contact* approximation. In the case of the mode ratio, however they give results that are often qualitatively different and at times also incorrect. These problems are expected to be compounded in systems of more delaminations with more complicated states of contact. Thus when accurate results are required, the simplified contact approximations should only be used as general bounds and as a first approximation of the regions of contact for the iterative solution of the *spring-contact* model.

Analysis of the energy release rate and mode ratio of the delaminations has revealed several key insights into the behavior of multiply delaminated systems. When delamination growth is considered, a discontinuity in the energy release rate and mode ratio is found when the delaminations reach the same length. This discontinuity leads to instantaneous shielding or amplification of the energy release rate, eliciting behaviors such as local snap-back and snap-through instabilities, hyperstrength, crack pull-along and crack arrest. All of these behaviors are strongly dependent on and controlled by the through-thickness spacing of the delaminations. The energy release rates of the delaminations are also amplified or shielded when the delaminations are not of the same length, again depending on the through-thickness positions of the delaminations. These effects show some similarity to the effects previously observed in the interaction of microcracks or of main cracks with clouds of microcracks in infinite media, which can represent damage in concrete and coarse grain ceramics (Hutchinson, 1987; Rose, 1986; Rubinstein, 1985; Kachanov, 1986; Brencich and Carpinteri, 1996). However in the problem considered here, strong modifications in the results and more complex behaviors are observed due to the finiteness of the structure.

The through-thickness positions of the delaminations also control the sensitivity of a system of equal length delaminations to length perturbations. When the delaminations are equally spaced the equality of length is stable (i.e. simultaneous growth of the delaminations) leading to a more ductile failure; when they are not, the equality of length is often, but not always, unstable resulting in a more brittle response (i.e. growth of one or a limited number of delaminations).

While the present study was limited to a system of only two unequal length delaminations, the proposed model could be applied to analyze systems with a general number of delaminations following the procedure described in Section 2. Behaviors similar to those of the two-delamination system are expected in a system with many delaminations, resulting in a macro structural response with a saw-tooth appearance, with repeated increases and decreases in critical load as the critical delamination tip grows with and past other delamination tips in the system. Different boundary and loading conditions from those studied here are expected to have a mostly quantitative effect on the results and can be easily solved using the same model and solution procedure. With minimal modification, friction acting in the regions of contact can also be considered. Its effect will be additional shielding of the energy release rate at the delamination tips.

Acknowledgements

MGA supported by Northwestern University. RM partially supported by the MIUR-Cofin2004 grant on "Problemi e modelli microstrutturali: applicazioni in ingegneria strutturale e civile" and the US Office of Naval Research through contract no. N00014-05-1-0098, administered by Dr. Yapa D.S. Rajapakse.

BNC supported by the US Army Research Office through contract number DAAD19-99-C-0042, administered by Dr. David Stepp.

Appendix A. Derivation of general solutions for system of coupled differential equations

In this appendix, the general solutions for the system of differential equations, Eqs. (7) and (8) are derived, for one free segment and for 2 and 3 beam segments in contact.

A.1. Single beam segment

For a single beam segment A the governing differential equations, Eqs. (7) and (8), are

$$\begin{aligned} &EI_A w_{A,xxxx} = 0, \\ &EA_A u_{A,xx} = 0 \end{aligned} \tag{A.1}$$

the general solutions of this system of equation is

$$\begin{aligned} &w_A(x) = C_1 + C_2 x + C_3 x^2 + C_4 x^3, \\ &u_A(x) = C_5 + C_6 x, \end{aligned} \tag{A.2}$$

where the C's are unknown constants of integration.

A.2. Two beam segments in contact

For two beam segments A and B in contact, the governing differential equations, Eqs. (7) and (8) are

$$\begin{aligned} &EI_A w_{A,xxxx} + k_{A,B}(w_A - w_B) = 0, \\ &EA_A u_{A,xx} = 0, \\ &EI_B w_{B,xxxx} - k_{A,B}(w_A - w_B) = 0, \\ &EA_B u_{B,xx} = 0, \end{aligned} \tag{A.3}$$

where $k_{A,B}$ is given by Eq. (5). Solutions of the form:

$$w_A(x) = A_1 \mathrm{e}^{\kappa x}, \qquad w_B(x) = A_2 \mathrm{e}^{\kappa x} \tag{A.4}$$

are sought. The resulting algebraic equation, determined by substitution of Eq. (A.4) into Eqs. (A.3) and subsequent elimination of A_1 or A_2 is

$$\kappa^4(\kappa^4 + 4\beta_{A,B}^4)\mathrm{e}^{\kappa x} = 0, \tag{A.5}$$

where

$$\beta_{A,B} = \sqrt[4]{\frac{k_{A,B}}{4}\left(\frac{1}{EI_A} + \frac{1}{EI_B}\right)}. \tag{A.6}$$

The relationship between the unknown constants A_1 and A_2 is

$$\frac{A_2}{A_1} = \frac{EI_B}{k_{A,B}}\kappa^4 + 1. \tag{A.7}$$

The 8 roots of Eq. (A.5) are

$$\kappa = 0, 0, 0, 0, \pm(1 \pm \mathrm{i}\beta_{A,B}), \tag{A.8}$$

where $\mathrm{i} = \sqrt{-1}$. The general solution of this system of differential equations is therefore

$$\begin{aligned} w_A(x) &= EI_A\,\mathrm{e}^{\beta_{A,B}x}(C_1\cos\beta_{A,B}x + C_2\sin\beta_{A,B}x) \\ &\quad + EI_A\,\mathrm{e}^{-\beta_{A,B}x}(C_3\cos\beta_{A,B}x + C_4\sin\beta_{A,B}x) + C_5x^3 + C_6x^2 + C_7x + C_8, \end{aligned} \tag{A.9}$$

$$\begin{aligned} u_A(x) &= C_9 + C_{10}x \\ w_B(x) &= EI_B\,\mathrm{e}^{\beta_{A,B}x}(C_1\cos\beta_{A,B}x + C_2\sin\beta_{A,B}x), \\ &\quad + EI_B\,\mathrm{e}^{-\beta_{A,B}x}(C_3\cos\beta_{A,B}x + C_4\sin\beta_{A,B}x) + C_5x^3 + C_6x^2 + C_7x + C_8 \end{aligned} \tag{A.10}$$

$$u_A(x) = C_{11} + C_{12}x.$$

A.3. Three beam segments in contact

The governing differential equations for three beam segments A, B and C in contact are

$$\begin{aligned} &EI_A w_{A,xxxx} + k_{A,B}(w_A - w_B) = 0, \\ &EA_A u_{A,xx} = 0, \\ &EI_B w_{B,xxxx} + k_{B,C}(w_B - w_C) = k_{A,B}(w_A - w_B), \\ &EA_B u_{B,xx} = 0, \\ &EI_C w_{C,xxxx} - k_{B,C}(w_B - w_C) = 0, \\ &EA_C u_{C,xx} = 0. \end{aligned} \tag{A.11}$$

The k's are given by Eq. (A.5). Solutions of the form

$$w_A(x) = A_1\,\mathrm{e}^{\kappa x}, \quad w_B(x) = A_2\,\mathrm{e}^{\kappa x}, \quad w_C(x) = A_3\,\mathrm{e}^{\kappa x} \tag{A.12}$$

are sought. The resulting algebraic equation for determination of κ is

$$\kappa^4(\kappa^8 + \alpha_{A,B,C}\kappa^4 + \gamma_{A,B,C})\,\mathrm{e}^{\kappa x} = 0, \tag{A.13}$$

where

$$\begin{aligned} \alpha_{A,B,C} &= k_{A,B}\left(\frac{1}{EI_A} + \frac{1}{EI_B}\right) + k_{B,C}\left(\frac{1}{EI_B} + \frac{1}{EI_C}\right), \\ \gamma_{A,B,C} &= k_{A,B}k_{B,C}\left(\frac{1}{EI_AEI_B} + \frac{1}{EI_AEI_C} + \frac{1}{EI_BEI_C}\right). \end{aligned} \tag{A.14}$$

The relationships between the unknown constants A_1, A_2 and A_3 are

$$\begin{aligned} \frac{A_2}{A_3} &= \frac{EI_C}{k_{B,C}}\kappa^4 + 1, \\ \frac{A_1}{A_3} &= \frac{EI_BEI_C}{k_{A,B}k_{B,C}}\kappa^8 + \left(\frac{1}{k_{A,C}}(EI_B + EI_C) + \frac{1}{k_{B,C}}EI_C\right)\kappa^4 + 1. \end{aligned} \tag{A.15}$$

The 12 roots of Eq. (A.13) are

$$\kappa = 0, 0, 0, 0, \pm(1 \pm \mathrm{i})\left(\frac{1}{2}\alpha_{A,B,C} \pm \frac{1}{2}\sqrt{\alpha_{A,B,C}^2 - 4\gamma_{A,B,C}}\right)^{1/4}. \tag{A.16}$$

The general solutions of the system of equations is therefore:

$$\begin{aligned}
w_A(x) &= C_1 + C_2x + C_3x^2 + C_4x^3 \\
&\quad + \rho_4 e^{\sqrt[4]{\rho_2}x}(C_5 \sin \sqrt[4]{\rho_2}x + C_6 \cos \sqrt[4]{\rho_2}x) + \rho_3 e^{\sqrt[4]{\rho_1}x}(C_7 \sin \sqrt[4]{\rho_1}x + C_8 \cos \sqrt[4]{\rho_1}x) \\
&\quad + \rho_3 e^{-\sqrt[4]{\rho_1}x}\left(C_9 \sin \sqrt[4]{\rho_1}x + C_{10} \cos \sqrt[4]{\rho_1}x\right) + \rho_4 e^{-\sqrt[4]{\rho_2}x}(C_{11} \sin \sqrt[4]{\rho_2}x + C_{12} \cos \sqrt[4]{\rho_2}x), \\
w_B(x) &= C_1 + C_2x + C_3x^2 + C_4x^3 \\
&\quad + \rho_6 e^{\sqrt[4]{\rho_2}x}(C_5 \sin \sqrt[4]{\rho_2}x + C_6 \cos \sqrt[4]{\rho_2}x) + \rho_5 e^{\sqrt[4]{\rho_1}x}(C_7 \sin \sqrt[4]{\rho_1}x + C_8 \cos \sqrt[4]{\rho_1}x) \\
&\quad + \rho_5 e^{-\sqrt[4]{\rho_1}x}(C_9 \sin \sqrt[4]{\rho_1}x + C_{10} \cos \sqrt[4]{\rho_1}x) + \rho_6 e^{-\sqrt[4]{\rho_2}x}(C_{11} \sin \sqrt[4]{\rho_2}x + C_{12} \cos \sqrt[4]{\rho_2}x), \\
w_C(x) &= C_1 + C_2x + C_3x^2 + C_4x^3 \\
&\quad + e^{\sqrt[4]{\rho_2}x}(C_5 \sin \sqrt[4]{\rho_2}x + C_6 \cos \sqrt[4]{\rho_2}x) + e^{\sqrt[4]{\rho_1}x}(C_7 \sin \sqrt[4]{\rho_1}x + C_8 \cos \sqrt[4]{\rho_1}x) \\
&\quad + e^{-\sqrt[4]{\rho_1}x}(C_9 \sin \sqrt[4]{\rho_1}x + C_{10} \cos \sqrt[4]{\rho_1}x) + e^{-\sqrt[4]{\rho_2}x}(C_{11} \sin \sqrt[4]{\rho_2}x + C_{12} \cos \sqrt[4]{\rho_2}x),
\end{aligned} \tag{A.17}$$

where

$$\begin{aligned}
\rho_1, \rho_2 &= \frac{1}{8}\alpha_{A,B,C} \mp \sqrt{\alpha_{A,B,C}^2 - 4k_{A,B}k_{B,C}\gamma_{A,B,C}}, \\
\rho_3 &= \frac{16EI_BEI_C\rho_1^2}{k_{A,B}k_{B,C}} - 4\frac{EI_Bk_{B,C} + EI_Ck_{B,C} + EI_Ck_{A,B}}{k_{A,B}k_{B,C}}\rho_1 + 1, \\
\rho_4 &= \frac{16EI_BEI_C\rho_2^2}{k_{A,B}k_{B,C}} - 4\frac{EI_Bk_{B,C} + EI_Ck_{B,C} + EI_Ck_{A,B}}{k_{A,B}k_{B,C}}\rho_2 + 1, \\
\rho_5 &= 1 - \frac{EI_C}{k_{B,C}}\rho_1, \quad \rho_6 = 1 - \frac{EI_C}{k_{B,C}}\rho_2.
\end{aligned} \tag{A.18}$$

Appendix B. Solutions for *n* equal length cracks

The solution for the system of n equal length cracks is determined by application of the boundary conditions Eq. (10) and continuity conditions Eq. (11). The general solutions for the intact beam segment, with index $k = 0$, and each of the beam segments, with indices $k = 1, \ldots, n+1$, in the delaminated region using the *unconstrained-contact* model are given by Eq. (A.2):

$$w_k(x) = C_{k,1} + C_{k,2}x + C_{k,3}x^2 + C_{k,4}x^3 \tag{B.1}$$

the $4(n+1)$ constants of integration are

$$\begin{aligned}
C_{0,1} &= C_{0,2} = 0, \quad C_{0,3} = \frac{1}{2}\frac{PL}{EI_0}, \quad C_{0,4} = -\frac{1}{6}\frac{P}{EI_0}, \\
C_{k,1} &= \frac{P}{6}(2a + L)(L - a)^2\left(\sum_{j=1}^{n+1}\frac{1}{EI_j} - \frac{1}{EI_0}\right), \\
C_{k,2} &= -\frac{P}{2}(L + a)(L - a)\left(\sum_{j=1}^{n+1}\frac{1}{EI_j} - \frac{1}{EI_0}\right), \\
C_{k,3} &= \frac{PL}{2}\sum_{j=1}^{n+1}\frac{1}{EI_j}, \quad C_{0,4} = -\frac{P}{6}\sum_{j=1}^{n+1}\frac{1}{EI_j}, \ k = 1, \ldots, n+1.
\end{aligned} \tag{B.2}$$

The constants for each of the segments in the cracked region, $C_{k,1}$, $C_{k,2}$, $C_{k,3}$, $C_{k,4}$, are identical, thus the deflections of the beam segments in the cracked region are the same. Therefore the other two contact approximations, the *constrained-contact* and the *spring-contact* yield the same solution.

The solution for the beam with n equal length cracks could also be determined by considering in the cracked region an equivalent intact beam with a reduced bending moment of inertia $I^* = \sum_{j=1}^{n+1} I_j$. This is also true in general under the assumptions of the *constrained-contact* model when the n cracks have arbitrary lengths. In this case, the beam is divided up into segments, each with a reduced bending moment of inertia determined by the sum of the bending moments of inertia of the delaminated sublaminates forming that segment.

The total potential energy Π of the system is

$$\Pi = \frac{1}{6}\frac{P^2L^3}{EI_0} - \frac{P^2a^3}{6}\left(\sum_{j=1}^{n+1}\frac{1}{EI_j} - \frac{1}{EI_0}\right). \tag{B.3}$$

Appendix C. Stability analysis of a cantilever beam with *n* equal length, equally spaced cracks

The stability of the equality of length of n equally spaced cracks in a cantilever beam is analyzed here using the assumptions of the *unconstrained-contact* model. If a positive perturbation Δa of crack m is considered, the energy release rate for crack m is

$$\frac{\mathscr{G}_m Eh}{P^2} = 6m(N-m)\left(\frac{a+\Delta a}{h}\right)^2\left(\frac{\chi_3 a^6 + 6\chi_1 a^3(a+\Delta a)^3 + 3\chi_2(a+\Delta a)^6}{\chi_1 a^3 + \chi_2(a+\Delta a)^3}\right), \tag{C.1}$$

where

$$\chi_1 = 6(m^4 - 2m^3N + m^2(N^2-3) + 3mN - N^2),$$
$$\chi_2 = 3(3m^2 - 3mN + N^2),$$
$$\chi_3 = -\frac{N^4}{3} + \left(\frac{2}{3}\chi_1 + \frac{4}{3}\chi_2\right)N^2 - \chi_1\left(\frac{\chi_2}{3} - 3\right),$$
$$N = n+1.$$

The energy release rate for each of the remaining n-1 cracks is

$$\frac{\mathscr{G}_i Eh}{P^2} = 6\frac{N^2}{N-2}\left(\frac{a}{h}\right)^2\left(\frac{\chi_4 a^6 + \chi_5 a^3(a+\Delta a)^3 + \chi_6(a+\Delta a)^6}{\chi_1 a^3 + \chi_2(a+\Delta a)^3}\right), \tag{C.2}$$

where

$$\chi_4 = \chi_1\left(-\frac{1}{3}N^2 + \frac{1}{3}\chi_2 + \chi_1 + 1\right),$$
$$\chi_5 = -\frac{2}{3}N^2(N^2 - \chi_2) + 2(\chi_2 + \chi_1\chi_2 + 3\chi_1),$$
$$\chi_6 = -\frac{2}{3}N^2\left(N^2 - \frac{5}{2}\chi_2\right) + 4\chi_2 + 5\chi_1.$$

The ratio of energy release rates, Eq. (C.1) by Eq. (C.2), taking the limit as $\Delta a \to 0$ is

$$\frac{\mathscr{G}_m}{\mathscr{G}_i} = \frac{m(N-m)(N-2)}{N^2}\left(\frac{\chi_3 + 6\chi_1 + 3\chi_2}{\chi_4 + \chi_5 + \chi_6}\right) = \frac{(n^2 - mn + 2n - m + 1 + m^2)(n-1)}{(-m^2 + mn + m - 1)(n+1)^2}. \tag{C.3}$$

The equality of length is stable if, for $n \geqslant 2$, $\mathscr{G}_m/\mathscr{G}_i < 1$. This condition is checked by verifying it at the extremum in terms of m and at the boundaries for $m = 1$, n. This yields

$$\frac{\mathscr{G}_{m_{ext}}}{\mathscr{G}_i} = \frac{3}{n+3}, \quad \frac{\mathscr{G}_1}{\mathscr{G}_i} = \frac{\mathscr{G}_n}{\mathscr{G}_i} = 1 - \frac{n}{(n+1)^2} \tag{C.5}$$

which are always less than 1 for $n \geqslant 2$.

If a negative perturbation Δa of crack m is considered then the energy release rate for crack m is

$$\frac{\mathscr{G}_m Eh}{P^2} = \left(\frac{a - \Delta a}{h}\right)^2 \frac{144N^2a^6}{(3(N-2)(a-\Delta a)^3 + (N+6)a^3)^2}. \tag{C.6}$$

The energy release rate for each of the remaining $n-1$ cracks is

$$\frac{\mathscr{G}_i Eh}{P^2} = 6\left(\frac{a}{h}\right)^2 \frac{\chi_7[(N+6)a^6 + 6(N-2)a^3(a-\Delta a)^3] + 9\chi_8(a-\Delta a)^6}{(3(N-2)(a-\Delta a)^3 + (N+6)a^3)^2}, \tag{C.7}$$

where

$$\chi_7 = (N^2 + 2N + 3),$$
$$\chi_8 = (N^3 - N + 2).$$

The ratio of energy release rates, Eq. (C.6) by Eq. (C.7), taking the limit as $\Delta a \to 0$ is

$$\frac{\mathscr{G}_m}{\mathscr{G}_i} = \frac{144N^2}{\chi_7(7N+6) + 9\chi_8} = \frac{3n+3}{2n+3}. \tag{C.8}$$

The equality of length is stable if, for $n \geqslant 2$, $\mathscr{G}_m/\mathscr{G}_i > 1$, which clearly is satisfied by Eq. (C.8). Thus the equality of length is stable for n equally spaced cracks.

Appendix D. Energy release rate expressions for a cantilever beam with two delaminations

The expressions for the normalized energy release rate for the upper and lower delamination, $\mathscr{G}_U$ and $\mathscr{G}_L$ for the cantilever beam of Fig. 5 are presented here. When the upper delamination is longer than the lower, $a_U > a_L$ Fig. 5a, the solution shows that there is contact along the delamination surfaces. The normalized energy release rates for the upper and lower delamination have been determined in closed form for the *unconstrained-* and *constrained-contact* models. The energy release rate for the *spring-contact* model is determined through the numerical solution of the problem and application of Eq. (9a).

For the *constrained-contact* model the energy release rates for $a_U > a_L$ are

$$\frac{\mathscr{G}_U Eh}{P^2} = 18\left(\frac{a_U}{h}\right)^2 \left(\frac{H_3(1-H_3)}{3H_3^2 - 3H_3 + 1}\right), \tag{D.1}$$

$$\frac{\mathscr{G}_L Eh}{P^2} = 18\left(\frac{a_L}{h}\right)^2 \left(\frac{H_5(1-H_3)(1-H_3-H_5)}{(3H_3^2 - 3H_3 + 1)(1 - 3(H_3+H_5)(H_5H_3+1) + 3(H_3+H_5)^2)}\right), \tag{D.2}$$

where $H_3 = h_3/h$ and $H_5 = h_5/h$. For the *unconstrained-contact* model the energy release rates for $a_U > a_L$ are

$$\frac{\mathcal{G}_U Eh}{P^2} = 18\left(\frac{a_U}{h}\right)^2 \left(\frac{H_3(1-H_3)(\gamma_1(a_U/h)^6 + \gamma_2(a_U/h)^3(a_L/h)^3 + \gamma_3(a_L/h)^6)}{(\gamma_4(a_U/h)^3 + \gamma_5(a_L/h)^3)^2}\right), \tag{D.3}$$

$$\frac{\mathcal{G}_L Eh}{P^2} = 18\left(\frac{a_L}{h}\right)^2 \left(\frac{(a_U/h)^6 H_5(1-H_3)^3(1-H_3-H_5)\gamma_6}{(\gamma_4(a_U/h)^3 + \gamma_5(a_L/h)^3)^2}\right), \tag{D.4}$$

where the constants $\gamma_1, \ldots, \gamma_6$ depend on the through-thickness positions of the cracks and are

$$\begin{aligned}
\gamma_1 &= (3H_3^2 - 3H_3 + 1)(H_3^2 + 3H_5^2 + 3H_3H_5 - 2H_3 - 3H_5 + 1)^2,\\
\gamma_2 &= 6H_5H_3^3(1-H_3-H_5)(H_3^2 + 3H_5^2 + 3H_3H_5 - 2H_3 - 3H_5 + 1),\\
\gamma_3 &= 3H_5^2H_3^2(1-H_3-H_5)^2(H_3^2 + H_3 + 1),\\
\gamma_4 &= -(3H_3^2 - 3H_3 + 1)(H_3^2 + 3H_5^2 + 3H_3H_5 - 2H_3 - 3H_5 + 1),\\
\gamma_5 &= -3H_5H_3^3(1-H_3-H_5).
\end{aligned} \tag{D.5}$$

When the lower delamination is longer than the upper delamination, $a_L > a_U$ Fig. 5b, the solution shows that there is opening along the lower delamination face, and no contact along the upper delamination face, namely the two upper beam segments have the same vertical deflection. Therefore, the *spring-* and *unconstrained-contact* models lead to the same solution. The *constrained-contact* model, which prevents opening, leads to a solution that is clearly incorrect in this regime. However, as will be seen later, it is a bound of the exact solution, which is useful for delamination configurations with more delaminations where the exact solution is not so obvious. The energy release rates are given by Eqs. (D.1)–(D.5) with the indices of crack positions and lengths reversed, $a_L \to a_U$, $a_U \to a_L$, $H_3 \to H_5$ and $H_5 \to H_3$.

When the delaminations have the same length, the energy release rate of each delamination when the delaminations propagate simultaneously, $\mathcal{G}_B$, is given by Eq. (12).

As for the case of equal length delaminations, Fig. 3, maps can be constructed for a general through-thickness distribution and lengths of the delaminations that show regions in which the energy release rate

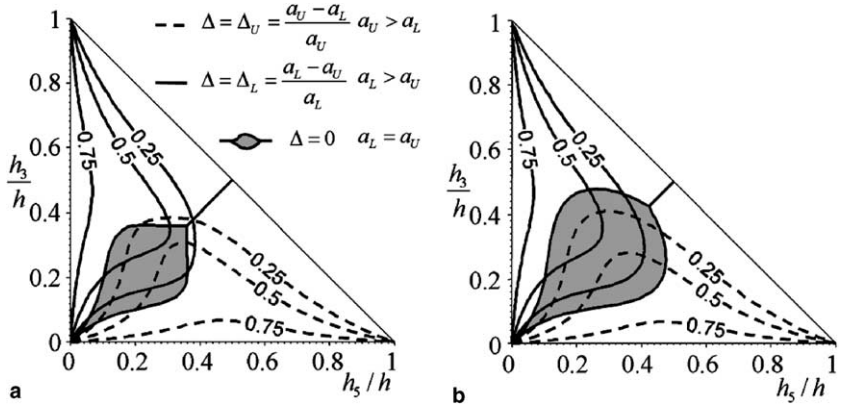

Fig. D.1. Maps of regions of different energy release rates for a system of two unequal length cracks (schematic of Fig. 5): (a) unconstrained model, (b) constrained model.

of one of the cracks is higher or lower than that of the other crack. Maps for the *constrained-* and *unconstrained-contact* models are shown in Fig. D.1.

The maps depend on the through-thickness position of the two cracks and incorporate contours of equal $\mathscr{G}$ of both cracks. The contours depend on the relative length of the two cracks. Dashed contours correspond to $\Delta_U = (a_U - a_L)/a_U$ and are to be used when $a_U > a_L$. Solid contours correspond to $\Delta_L = (a_L - a_U)/a_L$ and are to be used when $a_L > a_U$. The map in Fig. D.1a has been constructed using the *unconstrained-contact* model and the map in Fig. D.1b using the *constrained-contact* model. A more complicated map, depending also on the length of the cracks, can be constructed using the *spring-contact* model.

The shaded region in each figure refers to cracks of the same length, $\Delta_U = \Delta_L = 0$, and define configurations for which the energy release rate of each crack when the cracks propagate simultaneously, $\mathscr{G}_B$ given by Eq. (12), is maximum (the shaded region in Fig. D.1a coincides with that of Fig. 3). Points to the left or above the contour corresponding to the relative length of the two cracks define through-thickness distributions of the cracks for which the upper crack has the higher energy release rate. Points below or to the right of the contour define through-thickness distributions of the cracks for which the lower crack has the higher energy release rate. The evolution of the cracks can be followed in this diagram by updating the contour from that corresponding to the current Δ, to the configuration reached by the last crack growth event.

References

Andrews, G.M., Massabò, R., Cox, B.N., 2005. Frictional Interaction of Multiple Delaminations with Shear and Near Crack-Tip Deformation, Internal Report, University of Genova, Italy.

Brencich, A., Carpinteri, A., 1996. Interaction of a Main Crack with Ordered Distributions of Microcracks: A Numerical Technique by Displacement Discontinuity Boundary Elements. Int. J. Fracture 76 (4), 373–389.

Chan, S.K., Tuba, I.S., Wilson, W.K., 1970. On the finite element method in linear fracture mechanics. Eng. Frac. Mech. 2 (1), 1–17.

Hutchinson, J.W., 1987. Crack tip shielding by microcracking in brittle solids. Acta Metallurgica 35 (7), 1605–1619.

Hutchinson, J.W., Suo, Z.G., 1992. Mixed-Mode Cracking in Layered Materials. Adv. Appl. Mech. 29, 63–191.

Kachanov, M., 1986. On Crack–Microcrack Interactions. Int. J. Fracture 30 (4), 65–72.

Kanninen, M.F., 1973. Augmented double cantilever beam model for studying crack propagation and arrest. Int. J. Fracture 9 (1), 83–92.

Kanninen, M.F., 1974. Dynamic analysis of unstable crack propagation and arrest in the DCB test specimen. Int. J. Fracture 10 (3), 415–430.

Kerr, A.D., 1964. Elastic and Viscoelastic Foundation Models. J. Appl. Mech. 31, 491–498.

Larsson, P.L., 1991. On Multiple Delamination Buckling and Growth in Composite Plates. Int. J. Solids Structures 27 (13), 1623–1637.

Li, S., Wang, J., Thouless, M.D., 2004. The effects of shear on delamination in layered materials. J. Mech. Phys. Solids 52 (1), 193–214.

Massabò, R., Cox, B.N., 1999. Concepts for Bridged Mode II Delamination Cracks. J. Mech. Phys. Solids 47 (6), 1265–1300.

Pandey, R.K., Sun, C.T., 1996. Calculating strain energy release rate in cracked orthotropic beams. Journal of Thermoplastic Composite Materials 9 (4), 381–395.

Pavier, M.J., Clarke, M.P., 1995. Experimental-technique for the investigation of the effects of impact damage on carbon-fiber composites. Composite Science and Technology 55 (2), 157–169.

Remmers, J.J.C., de Borst, R., Needleman, A., 2003. A cohesive segments method for the simulation of crack growth. Computational Mechanics 31 (1–2), 69–77.

Rice, J.R., 1968. A Path Independent Integral and Approximate Analysis of Strain Concentration by Notches and Cracks. J. Appl. Mech. 35 (2), 379–386.

Rose, L.R.F., 1986. Microcracking interaction with a main crack. Int. J. Fracture 31 (3), 233–242.

Rubinstein, A.A., 1985. Macrocrack interaction with semi-infinite microcrack array. Int. J. Fracture 27 (2), 113–119.

Sridhar, N., Massabò, R., Cox, B.N., Beyerlein, I., 2002. Delamination Dynamics in Through-Thickness Reinforced Laminates with Application to DCB Specimen. Int. J. Fracture 118, 119–144.

Suemasu, H., 1993. Postbuckling Behaviors of Composite Panels with Multiple Delaminations. J. of Compos. Mater. 27 (11), 1077–1096.

Suemasu, H., Majima, O., 1996. Multiple Delaminations and Their Severity in Circular Axisymmetric Plates Subjected to Transverse Loading. J. of Compos. Mater. 30 (4), 441–463.

Sun, C.T., Pandey, R.K., 1994. Improved method for calculating strain energy release rate based on beam theory. AIAA Journal 32 (1), 184–189.
Suo, Z.G., 1990. Delamination Specimens for Orthotropic Materials. J. Appl. Mech. 57 (3), 627–634.
Suo, Z.G., Hutchinson, J.W., 1990. Interface crack between two elastic layers. Int. J. Fract. 43 (1), 1–18.
Wang, J., Qiao, P., 2004. Interface crack between two shear deformable elastic layers. J. Mech. Phys. Solids 52, 891–905.
Williams, J.G., 1989. End Corrections for Orthotropic DCB Specimens. Composite Science and Technology 35 (4), 367–376.
Yang, Q.D., Cox, B.N., 2004. Modeling damage evolution in laminated composites containing stress concentrators, International Journal of Solids and Structures in preparation for submission.
Zheng, S., Sun, C.T., 1998. Delamination Interaction in Laminated Structures. Eng. Frac. Mech. 59 (2), 225–240.